WAGENINGEN UNIVERSITY & RESEARCH
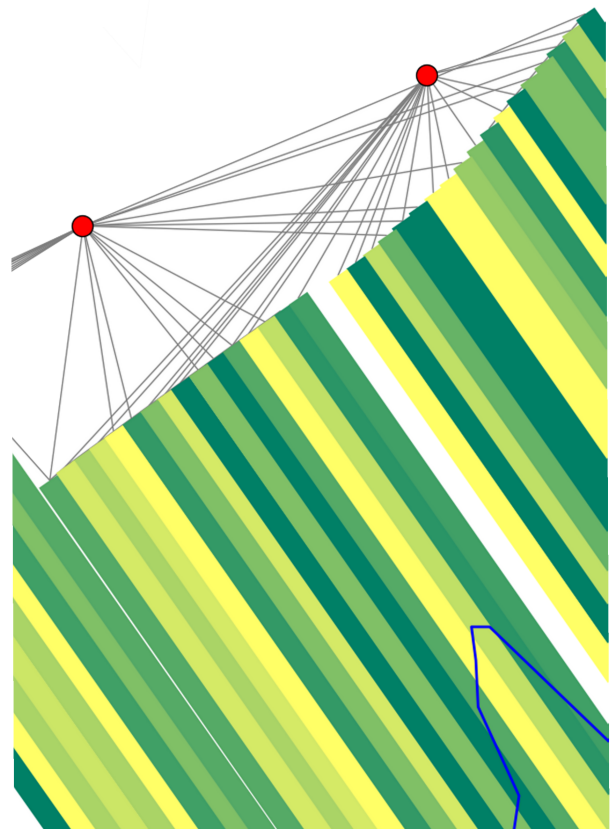
GEO-INFORMATION SCIENCE AND REMOTE SENSING

Capacitated Route Optimization In A Controlled Traffic Farming System

A Study On Route Planning With Minimal Soil Compaction In Agricultural Fields With Wet Areas

Author:
Yannick Mijnheer BSc.

Supervisor:
dr. ir. Sytze De Bruin

14th May 2018

WAGENINGEN
UNIVERSITY & RESEARCH

Capacitated Route Optimization In A Controlled Traffic Farming System

A Study On Route Planning With Minimal Soil Compaction
In Agricultural Fields With Wet Areas

Author:

Yannick MIJNHEER
Registration number 93 11 30 593 120

Supervisor:

dr. ir. Sytze DE BRUIN

A thesis submitted in partial fulfillment of the degree of Master of Science
at Wageningen University and Research Centre,
The Netherlands.

14th May 2018
Wageningen, The Netherlands

Abstract

Route optimization is an effective way to decrease soil compaction in agricultural fields. Important factors contributing to soil compaction are number of wheel passes, total weight of the working unit, and soil moisture content. This research aimed to determine an optimal route for capacitated agricultural operations over predefined field tracks given local differences in susceptibility to compaction (e.g. wet spots). In capacitated operations, the total weight of a working unit is variable, leading to a variable induced soil compaction. Together with known wet areas in a field, this creates room for route optimization. Route optimization is approached as a capacitated vehicle routing problem. Methods for generating weighted graphs representing an agricultural field and for calculating a (near-)optimal route through this graph were developed. The total cost of a route was calculated by a weighted sum objective function that expresses soil exposure to compaction in the unit weightmeters [m*kg]. The optimal route is the one with the lowest value of weightmeters. A Tabu search algorithm was implemented to heuristically search possible routes. The defined route optimization method found routes that were more optimal than the routes chosen by farmers, with far lower costs. Furthermore, in a small test field the Tabu search algorithm consistently found optimal solutions in 15.2% of the time of an exhaustive search method. In a follow-up study the suggested methods should be tested in practice, by planning near-optimal routes ahead of capacitated field operations. In the future, the proposed methods could be applied to farming machinery that work with GPS and predefined field tracks, to plan routes and thereby decrease induced soil compaction.

Keywords:

Contents

List of definitions

These are important words and their definitions, as they are used within this research paper.

Application operation	An agricultural operation where volume is added to the field (e.g. planting potatoes).
Capacitated field operations	Operations that involve the flow of material with capacity constraints to the load of material in the working units bunker.
Collection operation	An agricultural operation where volume is subtracted from the field (e.g. harvesting).
Depot	A facility for refilling (application operation) or unloading (collection operation) of the working units bunker, outside of the main field.
Distance capacity	The distance a working unit can work in normal field paths, starting with a full bunker, before reaching the bunker capacity.
Edges	Lines in a graph based on an agricultural field, representing the movement between two nodes.
Field path	A cultivated path in an agricultural field that is worked in one go, with a width equal to the smallest working width.
Headland	Part of the field that is left open on one side of the main field, to give space for turns between field paths.
Main field	The main part of an agricultural field, with the highest yield. The field minus the headlands.
Main field border	The border of the main field, the division of the main field and the headlands or field boundaries.
Multiplication factors	Factors in the objective function that weigh the different costs against each other.
Nodes	Points in a graph based on an agricultural field, representing field path ends (field nodes) and depot positions (depot nodes).
Route	The total route of a working unit during a capacitated agricultural field operation, starting at a depot, working all the field paths with necessary depot visits in between, and finishing back at a depot.
Spraypaths	Special field paths that are purposefully cultivated less than normal paths, to leave space for the tires of a spray machine.
Turning radius	The distance from the midpoint between the two rear wheels of a working unit and the center of the curvature, while the steerable wheels are at their maximum steering angle.
Working unit	One agricultural unit (e.g. a tractor with a potato planter), which is able to perform an agricultural operation on its own.

List of symbols

These are important symbols, with their unit and description, as they are used within this research paper.

α_{UT}	[°]	Total change of direction in a U-turn movement.
α_{XT}	[°]	Total change of direction in an X-turn movement.
C_d	[cm]	Distance capacity, the distance a working unit can work in normal field paths, starting with a full bunker, before the bunker is empty.
d_{UT}	[cm]	Distance of a U-turn movement parallel to the main field border.
d_{XT}	[cm]	Distance of an X-turn movement parallel to the main field border.
f_{HL}	[-]	Headland multiplication factor.
f_{UT}	[cm/°]	U-turn multiplication factor.
f_{SP}	[-]	Spray path multiplication factor.
f_W	[-]	Wet multiplication factor.
f_{XT}	[cm/°]	X-turn multiplication factor.
HL	[cm]	Distance costs for headland movements.
HL_{UT}	[cm]	Distance costs for U-turn movements.
HL_{XT}	[cm]	Distance costs for X-turn movements.
J	[m*kg]	Total cost of a route in weightmeters.
k	[-]	Index for the number of performed depot visits so far in route calculation.
k_{max}	[-]	Total number of depot visits in a route.
l	[-]	Distance driven since the last depot visit.
l_{max}	[-]	Total distance driven between the previous and the next depot visit.
MF	[cm]	Distance costs for main field movements.
NP_{dry}	[cm]	Distances driven in dry parts of normal paths.
NP_{wet}	[cm]	Distances driven in wet parts of normal paths.
r	[cm]	Minimal turning radius of center of working unit.
SP_{dry}	[cm]	Distances driven in dry parts of spraypaths.
SP_{wet}	[cm]	Distances driven in wet parts of spraypaths.
W	[kg]	Total weight of working unit.
W_{empty}	[kg]	Empty weight, total weight of working unit with empty bunker.
W_{full}	[kg]	Full weight, total weight of working unit with full bunker.
W_{bunker}	[kg]	Bunker weight, total weight capacity of bunker, W_{full} - W_{empty}.
WCM	[kg/cm]	Weight per centimeter, weight applied or collected from the field per worked centimeter in a normal field path.
$work_{NP}$	[cm]	Worked distance in normal paths since the last depot visit.
$work_{SP}$	[cm]	Worked distance in spraypaths since the last depot visit.

x

1 Introduction

1.1 Context and background

1.1.1 Soil compaction

The most serious environmental problem caused by conventional agriculture is soil compaction (McGarry, 2003). Globally, 68 million hectares of soil are degraded due to soil compaction, sealing and crusting. Almost half of this area, 33 million hectares, is situated in Europe, where the main reason for soil compaction is the use of heavy machinery (Oldeman, 1992). Since the Oldeman (1992) report, soil compaction has further increased, owing to a growing world population, growing pressure on food supplies, and ongoing trends towards larger, more powerful machines (Kutzbach, 2000; McPhee et al., 2015).

Soil compaction in arable fields has an indirect negative effect on nutrient uptake by plants through changes in root configuration (Gliński et al., 1990; Lipiec and Simota, 1994) and root-soil contact (Veen et al., 1992) and through decreased nutrient storage and supply (Hamza and Anderson, 2005). It also has an indirect negative effect on fuel consumption; increased bulk density through soil compaction requires increased pulling force for soil preparation, which wastes energy and increases fuel consumption (Gan-Mor and Clark, 2001). Furthermore, soil compaction increases water logging, water runoff, and soil erosion through decreased porosity, soil water infiltration, and water holding capacity of the soil, with unfavorable environmental pollutions as a result (Hamza and Anderson, 2005). The effects of soil compaction often show in the form of reduced crop establishment, growth, quality and yield (Soane and Van Ouwerkerk, 1994).

Solutions to these problems are often sought in reducing pressure on soils. Soil compaction can be directly reduced using lighter machines or larger tires (Greene and Stuart, 1985) with low inflation pressures (Douglas, 1994; Hetz, 2001). Tires with low inflation pressure can significantly decrease soil compaction (Boguzas et al., 2001; Ridge, 2002), whilst high-pressure tires increase soil compaction (Soane et al., 1982). However, almost all types of agricultural machines generate pressures above the recommended maximum limits to avoid soil compaction (Hetz, 2001), and working with low-pressure tires requires wider tires, enlarging the trafficked area (Tullberg et al., 2007).

A more effective solution is reducing machine traffic, or the number of wheel passes on a soil (Greene and Stuart, 1985). Research has shown that all soil properties become less favorable after the passage of a tractor (Chygarev et al., 2000). Decreasing machine traffic is suggested to be the most effective way to protect soils from structural soil compaction damage (Aliev, 2001).

Besides heavy machinery, soil moisture content largely affects compaction. Soil deformation does not only increase with the number of wheel passes, but also with the amount of soil moisture (Bakker and Davis, 1995). An increase in soil moisture content causes a decreased load support capacity of the soil (Lipiec et al., 2002). In other words; a constant soil pressure has a larger negative effect on a soil with a higher soil moisture content. Together, heavy machinery and soil moisture content form the most important soil compaction factors (Aliev, 2001). Therefore, heavy traffic in areas with relatively high soil moisture content should be minimized, since resulting compaction would be largest in these areas. Other soil properties also influence susceptibility to soil compaction, e.g. soil texture and bulk density (Horn and Fleige (2003); Duttmann et al. (2014)). These are however considered outside the scope of this research, due to their smaller influence.

1.1.2 Path planning

An increasingly popular way to reduce machine traffic is by controlled traffic farming (CTF). CTF is a system that separates trafficking lanes and crop beds, thereby providing permanent firmed tracks ideal for trafficking and permanent loose rooting zones ideal for cropping (Tullberg et al., 2007). CTF reduces machine traffic within the crop beds to a minimum, and restricts soil compaction to the trafficking lanes (Braunack et al., 1995). This leads to crop beds with improved soil structures, improved water infiltration and storage, and increased soil organic carbon content, compared to conventional crop beds (Li et al., 2009). In a study on the impact of CTF on 15 different crops in Australia, Tullberg et al. (2018) have found that CTF can decrease soil emissions of N_2O and CH_4 by 30 to 50%. A CTF system starts with path planning; it is necessary to define the paths that will consequently be used for trafficking.

1.1.3   Route planning

An efficient way to even further decrease trafficking, and thus soil compaction, is route planning. Route planning is the creation of routes by an algorithm that takes a combination of predefined costs into account (Spekken and de Bruin, 2013). By planning a route before travel, the efficiency of arable operations can be increased significantly (Taïx et al., 2003; Oksanen and Visala, 2007; Spekken and Molin, 2012). Palmer et al. (2003) found that route planning before travel could lead to an average reduction of 16% of the in-field distance traveled.

This study focuses on capacitated agricultural field operations. Capacitated operations are operations subject to capacity constraints of the bunker of a working unit. Due to these capacity constraints, the operation may have to be interrupted to visit a depot to either fill the bunker (in application operations) or empty the bunker (in collection operations). A depot is a facility for refilling or unloading of the working units bunker, depending on the operation. Agricultural field operations are often capacitated, e.g. harvesting, where the harvested crop has to be delivered to a depot, or fertilizing, where fertilizer has to be collected at a depot. In these capacitated operations, the non-working distance traveled is relatively high, which indicates a high potential benefit through route optimization (Jensen et al., 2015b). Furthermore, the total weight of the working unit depends on the load in the bunker, leading to a dynamic induced soil compaction.

Building on a CTF system with predefined tracks, finding an optimal route corresponds to a route optimization problem. The route optimization problem for capacitated agricultural field operations can be described as a capacitated vehicle routing problem (CVRP). Dantzig and Ramser (1959) introduced this problem for the first time, calling it a truck dispatching problem. The CVRP is an extended form of the more-common vehicle routing problem (VRP); the VRP is the problem of finding optimal collection or delivery routes from a depot to a number of places, where each place should be visited only once (Laporte, 1992). This is very similar to the traveling salesman problem (TSP), but instead of one salesman the VRP can work with several vehicles, therefore generating several separate routes. The CVRP extends the RVP by adding a maximum capacity to the vehicles, forcing them to return to the depot when their capacity is reached.

1.2   Current research

In 2014, de Bruin et al. described an approach to optimize the paths within an arable field, given only the field boundaries as input. Their path optimization service is called GAOS, and the objective of optimization is to avoid discontinuous field paths and inefficient turns between field paths. It also incorporates field margins, that might generate additional income through positive environmental impact and funding. It is successfully being used by farmers in the Hoeksche Waard, who plan their field paths and margins using GAOS, and use the planned paths in combination with auto-steering working units.

Oksanen and Visala (2007) also developed a path planning approach. This approach is focused on irregular shaped fields. The proposed algorithm divides a field into sub-regions, selects the sequence of those sub-regions, and generates a path that covers each sub-region. Hence, the algorithm incorporates route planning.

Zhou et al. (2014) proposed another method that is also based on division of a field into sub-regions. The focus of this approach is not on irregularly shaped fields, but on fields with obstacles. They also incorporated a route planning optimization connecting all the sub-regions in a specific order, though the routes are not optimized within those sub-regions.

Bochtis and Vougioukas (2008) developed an algorithmic approach for computing a route through parallel field paths. In this algorithm, the non-working distance traveled by a working unit performing an agricultural field operation is minimized. Non-working distance involves all distances traveled between two worked field paths or between a field path and a depot. The route traversing through all the field paths is expressed as a route through a weighted graph. Each node in this graph corresponds to a single field path, and each edge holds the weight assigned to the movement between field paths. The shortest tour through this graph resulted in the optimal path traversal order. In experimental results, they found that their algorithm could create routes that, when compared to the routes selected by farmers themselves, saved up to 50 % of the non-working distance traveled.

Jensen et al. (2015a) developed a route optimization algorithm specifically for capacitated field operations, thus incorporating intermediate visits to a depot. The optimization in their algorithm is also based on minimizing non-working traveled distance. This route optimization algorithm

incorporates half worked paths, and turns within the main field. During tests of the algorithm, they found savings in the non-working traveled distance from 15.7% up to 43.5%.

1.3 Problem definition

So far, we can conclude that heavy traffic in fields should be minimized, particularly in moist areas, in order to minimize further soil compaction. Path planning and applying a CTF system is a proper method to decrease soil compaction within the rooting zones. A logical next step to minimize overall soil compaction is route planning through these paths, especially for capacitated field operations due to the dynamic weight of the working unit.

In the last decades, numerous researches have been conducted on route planning through field paths in an agricultural field. However, no research has been found that focuses on soil compaction, and incorporates areas with higher vulnerability (e.g. wet areas) and the weight of the working unit. This thesis research has addressed agricultural in-field route planning, with a focus on minimizing soil compaction, whilst accounting for moist areas with higher vulnerability for soil compaction. The tackled problem was defined as follows; there is need for routes for capacitated agricultural field operations that minimize soil compaction by dealing with the two most important compaction factors, heavy machinery and soil moisture content.

1.4 Research objective and questions

The objective of this research is to determine an optimal route for capacitated agricultural operations over predefined field tracks given local differences in susceptibility to compaction (e.g. wet spots).

This objective has been achieved by answering the following research questions:

- What defines an optimal route for capacitated operations under spatially varying field circumstances?

- What optimization algorithm is best suited for finding such routes?

- Do test-case results of selected fields show an improvement over conventional routing?

2 Methods

This chapter explains in detail the methods used to tackle the research objective. The methods will be dealt with per research question.

2.1 Definition of an optimal route

A prerequisite for producing an optimal route is the definition of an optimal route. In this study, the aim of optimization is to reduce soil compaction in the field. An optimal route is therefore defined as a route with minimal induced soil compaction. During most agricultural field operations all paths in the field have to be worked. For capacitated agricultural field operations, this work may have to be interrupted to visit a depot. In this research the term "route" refers to the total route of a working unit during such an operation, starting at a depot, working all the field paths with possible depot visits in between, and finishing back at a depot.

Such a route consists of numerous movements. Every movement within a route is assigned a cost, related to the induced soil compaction during that movement. The sum of the costs of all movements in a route is a proxy for the induced soil compaction, and thus the optimality of a route. The process of planting potatoes is chosen as a proof of concept capacitated agricultural field operation for this research, although the methods are applicable to all capacitated agricultural field operations performed by a single working unit.

The considerations and choices made during the process of defining an optimal route are explained in full detail in the following sections.
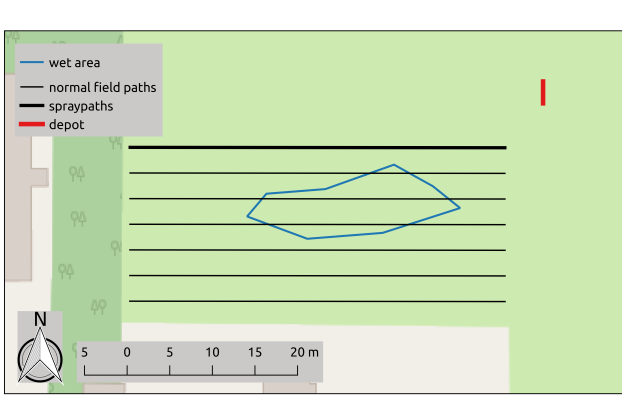
2.1.1 Graph presentation of fields

The costs for all possible movements in an agricultural field are stored in a weighted graph. Translating the movements in a field to a graph gives rise to many opportunities for algorithmic route calculations, e.g. shortest path calculations. Previous researches on route calculations within agricultural fields have been successfully performed by analyzing the costs of different routes within a weighted graph, and are used as sources of inspiration for this approach (e.g. Bochtis and Vougioukas (2008), Jensen et al. (2012)).

The created graph exists of nodes and edges. The nodes represent field path ends (field nodes) and depots (depot nodes), and the edges represent the movements of a working unit between those locations. Nodes store the coordinates of the position they represent, and identifiers for the field path or depot they represent. Edges store the costs ascribed to the movements they represent and the amount of work to be done during that movement if the edge represents a movement through a field path.

All edges are categorized as main field movements or headland movements. The main field is the main part of an agricultural field, containing the field paths, and delivering the highest yields. Main field movements are movements through field paths in the main field. Headlands are parts of the field left open around the main field, to give space for turns between field paths. Due to the numerous turns performed in headlands, the soil characteristics in headlands are less favorable than in the main field, instigating lower yields. Typically, a field consists of two separate headlands on two opposite sides of the field. The methods in this study do not accept fields with more than two headlands. Headland movements can take place between two path ends on the same side of the field or between a path end and a depot. The nodes representing field path ends also represent the border between main field and headland. All movements in the headlands are considered non-productive in this study, i.e. the working unit does not perform an operation during these movements. In practice, operations are commonly performed in the headlands after (in application operations) or before (in collection operations) the operation is performed for the entire main field, creating new field paths in the headlands. Due to the smaller size and importance of the headlands, route calculations through field paths in headlands are considered outside the scope of this study.

Necessary input data for the creation of this graph are the exact locations of field paths, depots, and wet areas within an agricultural field. For the field paths, it is necessary to know which of the paths are spraypaths. Figure 1a shows a map with these data for a simple agricultural field, with only seven paths and one depot. A relatively large wet area is defined in the main field. This hypothesized field, Test field 1, is used for testing purposes in a later stage of this research. Figure 1b shows the graph version of the same field.

(a) Map of Test field 1.
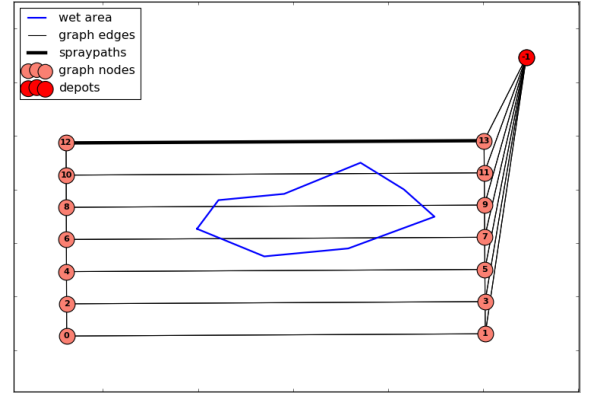
(b) Representation of graph of Test field 1.

Figure 1: A schematic map of Test field 1, a hypothetical agricultural field, and a representation of the weighted graph based on the same field.

Edges created to represent the main field movements are based directly on the field paths, given as input data. However, the input data do not contain information on the paths followed during headland movements. Edges created to represent the movements in the headlands are therefore based on the node positions. All nodes on one side of the main field are connected to each other with edges, representing all possible headland movements. This is based on the assumption that a working unit has to traverse a path in the main field to move from one side of the field to the other side of the field. In the example shown in Figure 1b. this leads to headland edges between nodes 0, 2, 4, 6, 8, 10, and 12 on one side, and nodes -1, 1, 3, 5, 7, 9, 11, and 13 on the other side of the field.

This means that a working unit has three possible movements when it is positioned at a field node. It can move through the field path towards the other side of the main field, it can move to a different field node on the same side of the field, or it can move to a depot positioned on that side of the field. When a working unit leaves a depot it can only move to a field node on the side of the field where the depot is at.

2.1.2   Soil compaction criterion

Distance traveled and weight of the working unit are the two overarching factors to be minimized in this research, especially in the wet areas, which are more susceptible to soil compaction. A larger weight of the working unit, as well as more distance traveled in the field, causes larger soil compaction.

The costs stored in the graphs edges represent the costs for traveled distance of a movement. These distance costs are made up of five types of distances. These different types were identified to give different costs to different types of movements, depending on the induced soil compaction. The five types of distances are distance in the main field, distance in spraypaths, distance in wet areas, distance in headlands, and turns. The distance cost for distance in the main field is taken as starting point; the costs of the other four types of distances are weighed against this cost using multiplication factors. For every edge these five distance costs are summed and stored.

The costs for the weight of the working unit is incorporated on the fly during the route calculations. It is not stored in the edges, because it cannot be known in advance since it depends on the route taken during the operation. It changes during the process of working field paths. During a collection operation the weight increases, and during an application operation the weight decreases when working a path. Owing to this change of weight during an operation, the cost for the weight of a working unit cannot be stored in the edges as a constant value. Planting potatoes, which is chosen as a proof of concept operation during this research, is an example of an application operation.

During the route calculations, the costs stored in the graphs edges are multiplied with the instantaneous weight of the working unit. Summing these values for an entire route leads to a total soil compaction value, defined in weightmeters [m*kg]. This cost unit is proposed upon consultation of farmers in the Hoeksche Waard. The weightmeters of a route are used as a soil compaction criterion, making different routes comparable. The optimal route is the route with the least weightmeters. The weightmeters of a route are calculated using a weighted sum objective

function, as will be explained in section 2.1.8. The following sections will first describe how the distance costs are computed, based on simplifications of actual movements.

2.1.3 Distance in the main field

Most distance is traveled in the main field, as the main field comprises the largest part of a field. Therefore, the costs for these distances are taken as a starting point. They are simply calculated as the distance traveled through the main field, or through the field paths. Unfortunately these costs are most difficult to minimize, since all paths have to be worked exactly once. The distance driven in the main field is thus at least equal to the sum of the lengths of all paths in the main field. The main field distance increases if the working unit has to visit a depot, and has to pass through the main field on its way there, without working. The path passed in such a case will be traversed at least twice during this route. This demonstrates how minimization of the main field distance is involved.

The distance driven in the main field is composed of distance in normal paths and distance in spraypaths, and of distance in dry areas and distance in wet areas. In spraypaths and in wet areas the costs are multiplied with an appropriate multiplication factor.

2.1.4 Distance in spraypaths

Most field paths are identified as normal paths. Some paths are however spraypaths. These paths are purposefully cultivated less than normal paths, to leave space for the tires of a spray machine. In a CTF system, these paths provide easy traffic through the main field. Consequently, these paths produce lower yields. Costs for distances traveled through spraypaths are therefore lower than costs for distances through normal paths. This is achieved by multiplying distances through spraypaths with a spraypath multiplication factor, f_{SP} [-]. The value of this factor is user-defined, and depends on the amount of work done in spraypaths. It is common use to plant half the amount of a normal path in a spraypath, as explained by farmers from the Hoeksche Waard. This leaves more space for the spray machine to traverse the path, whilst still producing yield. In such cases f_{SP} would be set to 0.5, making costs for distances in spraypaths half as heavy as costs for distances in normal paths.

2.1.5 Distance in wet areas

Besides normal paths and spraypaths, the distances in the main field are classified as distances through dry or wet areas. As areas with higher soil moisture content are more susceptible to soil compaction, the distance costs through wet areas are considered higher than distance costs through dry areas. This is where the input wet areas are used. These input files come in the form of shapefiles, indicating areas within the main field that are considered wet, in comparison to the rest of the field. Field paths, both normal paths and spraypaths, can intersect with these wet areas. The distance cost for the intersecting part of a field path is multiplied with a wet multiplication factor, f_W [-]. This factor is again user-defined, because the wetness of the wet areas depends largely on the season, and can be different for each field. However, it should always have a value higher or equal to one (cost of distances through dry areas).

The costs stored in field edges, representing movements through field paths are calculated using Equation 1. In this equation, all distances in the main field come together to one total cost value, MF [cm], calculated for every field edge. NP_{dry} and NP_{wet} are the distances driven in dry and wet parts of normal paths [cm], respectively, and SP_{dry} and SP_{wet} are the distances driven in dry and wet parts of spraypaths [cm], respectively. f_{SP} is the spraypath multiplication factor [-], and f_W is the wet multiplication factor [-].

$$MF = \underbrace{\left(NP_{dry} + f_W\,NP_{wet}\right)}_{\text{normal paths}} + \underbrace{f_{SP}\left(SP_{dry} + f_W\,SP_{wet}\right)}_{\text{spraypaths}} \quad \text{[cm]} \tag{1}$$

2.1.6 Distance in headlands and turns

Headland movements take place between two field nodes, and between field nodes and depot nodes. Due to the large number of movements in headlands during field operations, these parts of the route offer much room for reduction of traffic, and thus reduction of soil compaction. The distance costs for headland movements are calculated separately from distance costs for main field movements, because of the lower yield and importance of headlands in agricultural fields. By separating the costs, the costs for headland movements can be weighed against the costs for main field movements with a multiplication factor. In most cases in this study the headland movements got a lower cost than the main field movements.

Almost all headland movements require a turning motion. Movements between two field paths require a turn of at least 180 degrees. In this research, all edges representing headland movements are classified as movements that can be made using a single bend, referred to as U-turns, and movements that require reverse driving, which are known as fishtail turns, or X-turns. Figure 2 illustrates these two types of turns. A U-turn is preferred over an X-turn for minimizing soil compaction because of the smaller traversed distance and less maneuvering Sabelhaus et al. (2013). An X-turn is therefore only used when a U-turn is not possible. Other possible turns, such as omega turns, are left out of this research for sake of simplicity. They could however be implemented in a similar way as X-turns.

Feasibility of U-turns is restricted by the minimal turning radius of the working unit. If the length of a headland movement is shorter than twice the turning radius, a U-turn is not possible, and an X-turn is necessary. Which of the two (U-turn or X-turn) will be executed is thus determined by the turning radius of the working unit and the length of the headland movement.
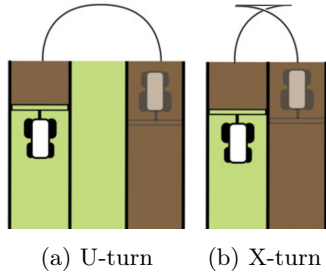

(a) U-turn (b) X-turn

Figure 2: Considered headland turns between two field paths.

In this thesis, edges that connect field paths to depots are always modeled as U-turns. This is because the depots have unknown orientation. It was therefore impossible to determine what would be the true path between a depot and the main field. For simplicity it is assumed that the depots can be reached from the field paths in a straight line, and vice versa, so that X-turns are not necessary.

The costs of headland movements as stored in the headland edges comprise a distance part and a turn factor. The distance part is an approximation of the length of the path of the actual movement. This approximation of the distance uses the distance of the actual movement parallel to the main field border, the total change of direction during the actual movement, and the turning radius of the working unit. The turn factor is added for two reasons. The first is to compensate for the extra soil compaction caused by turning movements compared to straight movements. The second is to give a higher preference to one of both types of turns, depending on field characteristics or on future research on differences in impact. The turn factor is based on the approximated total change of direction of the represented headland movement. In order to calculate the costs for headland movements it is thus necessary to know the distance parallel to the main field border d [cm], the total change of direction α [°], and the turning radius of the working unit r [cm]. The turning radius r is constant throughout a route, whereas d and α are calculated for every movement.

The distance parallel to the main field border is calculated using the field nodes, representing the field path ends. During a headland movement between two field paths, several field paths can be passed. The distance traversed during this movement parallel to the main field border is calculated as the sum of the distances between the path ends of all passed field paths. This is equal to the sum of the distances between the passed nodes. For a movement between a field node and a depot node, the distance d is assumed to correspond to the
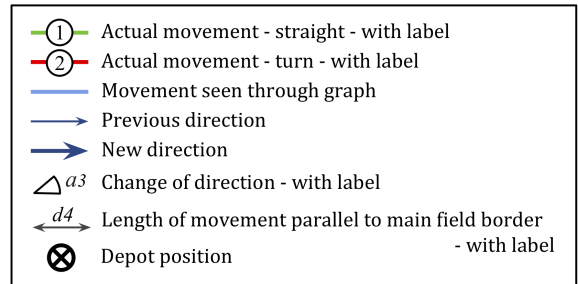

Figure 3: Legend for Figures 4, 5, 6, and 7.

euclidean distance between the two.

Total change of direction is calculated using the original driving direction, the change of direction within the headland movement, and the final driving direction. For headland movements between two field paths, the original and final driving directions are parallel, but exactly opposite. The change of direction is thus at least 180°. It can be larger if the approached main field border is curved, due to field paths with different lengths, as depicted in Figure 4. For movements between a field path and a depot, the direction of the working unit at the depot is unknown; for these movements α is simply the difference between the direction in the field path and the direction of the edge inserted between the field path and the depot.
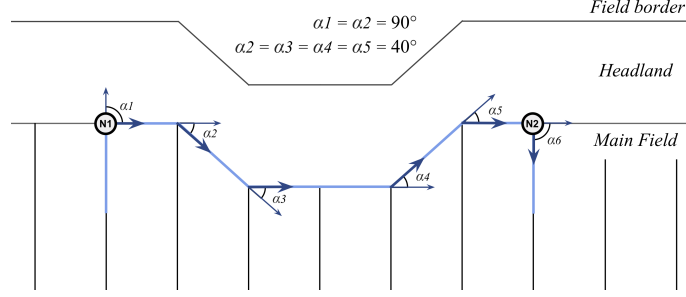

Figure 4: Schematic representation of a headland where the total change of direction in a movement between N1 and N2 is larger than 180°, equal to $2 \times 90 + 4 \times 40 = 340°$. See Figure 3 for the legend.

U-turns A typical U-turn movement is detailed in Figure 5. In this example, a working unit leaves a field path on the left side, makes a turning movement in the headland (1), followed by a straight movement (2), and a second turning movement (3), after which it re-enters the main field in a different field path on the right side. The distance parallel to the main field border is labeled d. The approximated changes of direction of the two turning movements are labeled $\alpha1$ and $\alpha2$, and are both equal to 90°.

Figure 5: Schematic representation of a typical U-turn movement between two field paths. See Figure 3 for the legend.

Equation 2 shows how the distance costs for a headland movement classified as U-turn are calculated. In this equation, d_{UT} is the distance of a U-turn movement parallel to the main field border [cm], r the turning radius of the working unit [cm], α_{UT} the total change of direction of the U-turn movement [°], and f_{UT} the U-turn multiplication factor [-].
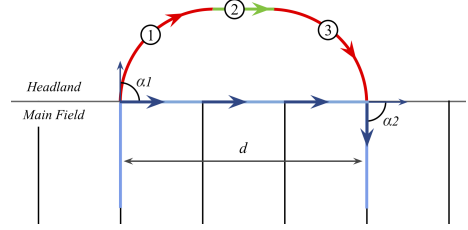
$$HL_{UT} = \underbrace{d_{UT} + (\pi - 2)r\frac{\alpha_{UT}}{180}}_{\text{distance part}} + \underbrace{f_{UT} * \alpha_{UT}}_{\text{turn factor}} \quad [\text{cm}] \qquad (2)$$

The calculation of the distance part can be explained by means of Figure 5. For the example in this figure, α_{UT} is the sum of $\alpha1$ and $\alpha2$, which is 180°. The length of both turning movements (1 and 3) together is calculated with $2\pi r \frac{\alpha_{UT}}{360}$, or $\pi r \frac{\alpha_{UT}}{180}$. For the example, with $\alpha_{UT} = 180°$, this is simply πr.

The length of the straight movement (2) is equal to d minus the lengths of movements 1 and 3 parallel to the main field border. With $\alpha1 = \alpha2 = 90°$, these lengths are equal to the turning radius r. The length of movement 2 is thus $d - 2r$.

The total distance traveled in the movement in Figure 5 is therefore $d - 2r + \pi r$, or $d + (\pi - 2)r$. This formula has been generalized to scale with the total change of direction, by multiplying the second part of the formula with $\frac{\alpha_{UT}}{180}$, leading to the distance part as it is in Equation 2. This is a simplification based on the simple example U-turn in Figure 5. The formula applies to U-turns with α_{UT} close to 180°, or fields with close to straight main field borders. Calculating a more generically applicable equation was considered beyond the scope of this thesis research.

X-turns A typical X-turn movement is detailed in Figure 6 . In this example, a working unit leaves a field path on the left side, makes a turning movement in the headland (1), followed by a straight movement (2), and a second turning movement (3), after which it re-enters the main field in a different field path on the right side. The distance parallel to the main field border is labeled d. The approximated changes of direction of the two turning movements are labeled $\alpha 1$ and $\alpha 2$, and are both equal to 90°.

Figure 6: Schematic representation of a typical X-turn movement between two field paths. See Figure 3 for the legend.

Equation 3 shows how the distance costs for a headland movement classified as an X-turn is calculated. In this equation, d_{XT} is the distance of an X-turn movement parallel to the main field border [cm], r the turning radius of the working unit [cm], α_{XT} the total change of direction of the X-turn movement [°], and f_{XT} the X-turn multiplication factor [-].

$$HL_{XT} = \underbrace{2r - d_{XT} + \pi r \frac{\alpha_{XT}}{180}}_{\text{distance part}} + \underbrace{f_{XT} * \alpha_{XT}}_{\text{turn factor}} \quad \text{[cm]} \tag{3}$$

The movement is very similar to the U-turn movement in Figure 5. The calculation of the distance part is therefore also very similar to the calculation for the U-turn. The main difference is however that the two turning movements (1 and 3) in Figure 6 overlap, and that the straight movement (2) is in the opposite direction, performed in reverse. For the example in this figure, α_{XT} is the sum of $\alpha 1$ and $\alpha 2$, which is again 180°. The length of both turning movements (1 and 3) together is calculated with $2\pi r \frac{\alpha_{UT}}{360}$, or $\pi r \frac{\alpha_{UT}}{180}$. For the example, with $\alpha_{UT} = 180°$, this is simply πr.

The length of the reverse movement (2) is however different. It is not equal to d minus the lengths of movements 1 and 3 parallel to the main field border, as with the U-turn. Instead, it is equal to the opposite; the lengths of the movements 1 and 3 parallel to the main field border minus d. The length of movement 2 in Figure 5 is thus $2r - d$.

The total distance traveled in the movement in Figure 6 is therefore $2r - d + \pi r$. This formula has been generalized to scale with the total change of direction, by multiplying the third part of the formula with $\frac{\alpha_{UT}}{180}$, leading to the distance part as it is in Equation 3. This is a simplification based on the simple example X-turn in Figure 6. The formula best applies to X-turns with α_{UT} close to 180°, or fields with close to straight main field borders. Calculating a more generically applicable equation was considered beyond the scope of this thesis research.

Movements to/from depot A typical headland movement to visit a depot is shown in Figure 7. In this example, a working unit leaves a field path on the left side, makes a small turning movement into the headland (1), followed by a straight movement (2), after which it arrives at the depot on the right side. The distance d does not represent the distance parallel to the main field border, but rather the euclidean distance between the path end of the field path and the depot position. The approximated changes of direction of the turning movement is labeled α.

This movement, as well as all other possible movements between a field path and a depot, is classified as a U-turn movement. The calculations for the costs of this movement are exactly the same as with a U-turn movement, as shown in Equation 2, except for the fact that d_{UT} in these cases represents the euclidean distance between the field path end and the depot position, as explained earlier.

Figure 7: Schematic representation of a typical U-turn movement between two field paths. See Figure 3 for the legend.

The total costs of headland movements can be calculated with Equation 4, which combines Equation 3 and Equation 2, and multiplies them with the
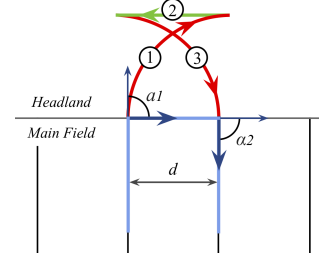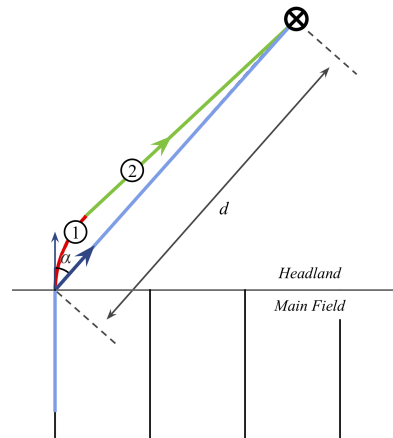
headland multiplication factor f_{HL}[-]. The headland factor is incorporated to make the influence of headland movements on the total costs of a route variable. Due to the lower yields of headlands, compared to the main field, the headlands are often regarded as less important than the headlands. CTF systems are also focused on decreasing soil compaction in the main field (Bochtis and Vougioukas, 2008). Therefore, the headland factor is most often set smaller than 1, to make the influence of headland movements on the total costs of a route smaller than the influence of main field movements.

$$HL = f_{HL}\big(HL_{UT} + HL_{XT}\big) \quad \text{[cm]} \tag{4}$$

2.1.7 Weight

A necessity for calculating the weightmeters of a route is to know the total weight of the working unit at every moment, depicted by W [kg]. Full weight W_{full} [kg], empty weight W_{empty} [kg], and distance capacity C_d [cm] are input data for the weight calculation. The full and empty weight are the total weight of the working unit with a full and empty bunker, respectively. The distance capacity represents the distance that a working unit can work in normal paths before the bunker is empty, when starting with a full bunker. From these input data, the decrease in weight per distance worked in normal paths, WCM [kg/cm], is calculated. WCM is an abbreviation of **w**eight per **c**enti**m**eter, and is calculated using Equation 5. WCM is different for distance worked in spraypaths, since the amount of work done in spraypaths is different compared to normal paths. Therefore, the distance worked in spraypaths is first multiplied with the spraypath multiplication factor, f_{SP} [-]. The the total weight of the working unit at the start of a route and after visiting a depot is assumed to be equal to the full weight W_{full}. This leads to Equation 6, where W is the total weight of the working unit [kg] and $work_{NP}$ and $work_{SP}$ [cm] are the worked centimeters since the last depot visit in normal paths and spraypaths respectively.

$$WCM = \big(W_{full} - W_{empty}\big)/C_d \quad \text{[kg/cm]} \tag{5}$$

$$W = W_{full} - WCM\big(work_{NP} + f_{SP}work_{SP}\big) \quad \text{[kg]} \tag{6}$$

2.1.8 The objective function

The six factors distance in the main field, distance in the headlands, distance in spraypaths, distance in wet areas, turns, and weight are summarized in the weighted sum objective function J, where J equals the total weightmeters of a route [m*kg]. J is a combination of Equations 1, 4, and 6. The equation used to calculate J is shown in Equation 7. Figure 8 gives a schematic overview of this weighted sum objective function.

$$J = \frac{1}{100} \sum_{k=0}^{k=k_{max}} \left(\sum_{l=0}^{l=l_{max}} \big(W(MF + HL)\big) \right) \quad \text{[m*kg]} \tag{7}$$

In this equation, k is an index for the number of performed depot visits so far, with k_{max} being the total number of depot visits in a route. l represents the distance driven since the last depot visit [cm], with l_{max} being the total distance driven between the previous and the next depot visit. When $l = 0$, the weight W is always equal to W_{full}. When $l = l_{max}$, the weight W is always close or equal to W_{empty}. With every depot visit in a route, k is incremented with 1 and l is reset to 0. For every centimeter in a route, $W(MF + HL)$ is calculated, and added to the grand total J. After dividing the total sum through 100, J is equal to the total weightmeters of a route [m*kg].
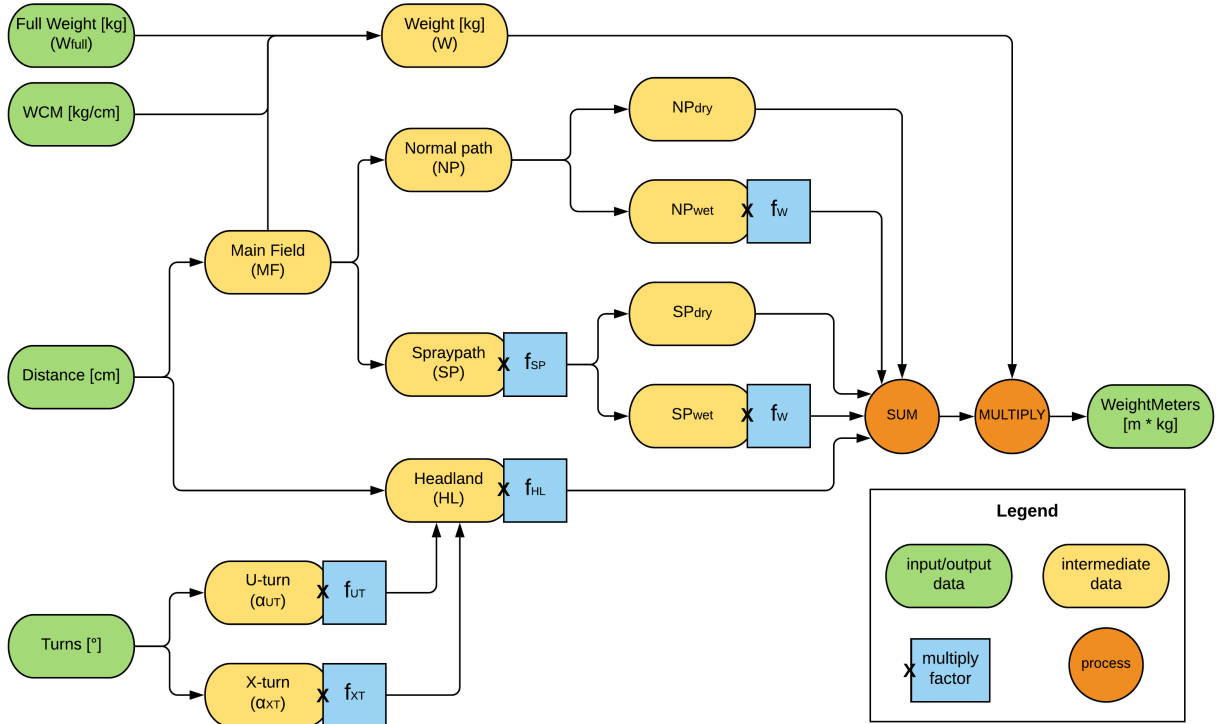
Figure 8: Schematic overview of Equation 7. The multiplication factors weigh the different costs against each other, and correct for differences in unit. The weight (W) is a dynamic cost, calculated on the fly during route calculations.

2.1.9 Implementation

This objective function is implemented in a Python script. Input data consists of two shapefiles; one with lines of field paths and lines at depot positions, and one with shapes of wet areas within an agricultural field. For the field paths, it is necessary to know which of the paths are spraypaths. Figure 1a shows a map with these input data for Test field 1. Other important input data is a path order, which defines an ordered set of field paths to be worked. The created script automatically generates a graph from these data, using the Python package *NetworkX*.

For every path line, two nodes representing the path ends are added to the graph, with stored coordinates of these path ends (field nodes). For every depot line a node representing the depot position is added, with stored coordinates of the center of this line (depot nodes).

Edges are created between field nodes representing the same field path, between neighboring field nodes on the same side of the field, and between field nodes and depot nodes on the same side of the field, if present. For all of these edges, information is stored on the position (headland or main field), whether it represents a move through a spraypath (true or false), whether it represents a move through a wet area (true or false), and the euclidean distance between the two nodes it connects.

This first graph is used as a starting point for the calculations of the actual cost graph. The edges represent all possible paths that a working unit can follow. The cost graph is a simpler graph, stored as a Python dictionary. The cost graph contains the same nodes as the first graph, but it is a fully connected graph, i.e. all nodes are connected with each other. Furthermore, it is a directed cost graph, which means that an edge can have different costs for both directions.

The first graph is used to calculate the shortest route between each pair of nodes in the cost graph. This is why the NetworkX package was used for the first graph; the NetworkX package has a Dijkstra shortest path calculation built in. For every combination of nodes in the cost graph, the edges traversed in this shortest path are stored, to present the actual path followed between two nodes. In these shortest path calculations, the distances through spraypaths get 20% of the weight of normal field paths. This ensures that spraypaths are chosen when the main field needs to be traversed without working, e.g. when a depot visit is necessary.

The information stored in the edges and nodes of the first graph is used to calculate distance costs for every possible movement, using Equations 1 and 4. This whole process takes place autonomously; in order to calculate the costs between two nodes in weightmeters, the Python script identifies which part of the shortest route takes place in a headland, what type of turn is necessary, what part takes place in the main field, and what the costs are for every part of the movement. The total distance costs are stored in the edges of the new cost graph.

For edges representing movements through the main field, where work is performed, the cost graph not only stores the distance costs but also the influence that the performed work has on the total weight of the working unit.

The combination of changing weight during work done in field edges and the fact that these edges can intersect with wet areas requires the cost graph to be directed. Due to the changing weight, the exact location where a field edge intersects with a wet area has a large influence on the total cost in weightmeters of working an edge. The total costs thus depend on the direction in which the edge is worked. These total costs of working an edge through a wet area are also calculated automatically.

The cost graph is used to calculate the weightmeters of an entire route, using Equation 7, by calculating the weight for every moment within a route and multiplying the stored distance costs with the weight of the working unit. These costs are calculated instantaneously while the route is generated.

A total route is stored as an ordered list of visited nodes. A route always starts and finishes at a depot node. Starting in a depot node, the route is based on the input path order. The paths defined in the path order, as well as the shortest routes between these paths, are stored in a list of the total route. A consecutive path in the path order is always added to the list starting with the path node on the same side of the field as where the previous node in the route was.

A depot visit is always and only added to the route if either the next path in the given order cannot be incorporated in the route anymore without reaching the distance capacity, C_d, or because all paths from the path order are already incorporated in the route. When a depot visit is necessary the number -999 is stored in the total route. This number functions as a label, to distinguish the working process from the depot visit. A field edge incorporated in the route between the label -999 and a depot node is thus not worked, but simply traversed to reach the depot. After adding this label, a move to the depot that can be reached with the least costs is added to the route.

An example of a part of a route through the graph of Test field 1, shown in Figure 9, is [-1, 1, 0, 2, 4, 5, 7, 9, 8, -999, 10, 12, 13, -1]. In this example, the route suggests that a working unit would start at depot node -1, work three paths in the main field, finishing at node 8, and from there move back to the depot, traversing the main field through the spraypath.

The weightmeters of all moves in the generated route are calculated and summed up on the fly. The two outputs of the Python script are a route, stored as a list of nodes and labels, and the costs of the route in weightmeters, stored as an integer value.

2.1.10 Testing

So far, the created Python script takes an agricultural field with or without defined wet areas as input, together with a number of defined input variables and a given path order, to calculate the best route and the costs in weightmeters. This Python script was tested on a hypothetically small test field, called Test field 1, with only seven paths in the main field. Its small size made it possible to perform an exhaustive search approach to find the true optimal route. Figure 9 shows the graph created based on Test field 1, with the nodes projected according to the coordinates of the path ends and the depot positions.
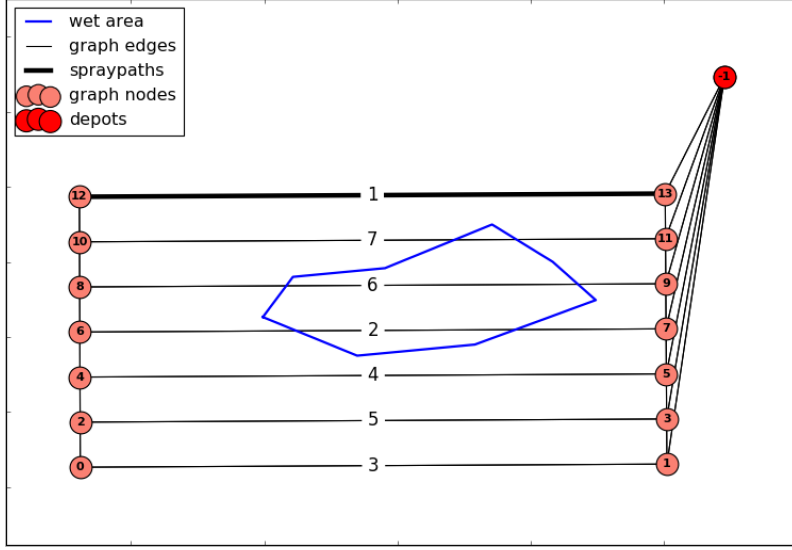
Figure 9: Graph representation of Test field 1, with labels in field edges representing path order of test route.

The graph of Test field 1 was used to test the influence of the multiplication factors in the objective function. The objective function has five multiplication factors incorporated as input variables; the spraypath multiplication factor f_{SP} [-], the wet multiplication factor f_W [-], the headland multiplication factor f_{HL} [-], the U-turn multiplication factor f_{UT} [cm/°], and the X-turn multiplication factor f_{XT} [cm/°]. Every multiplication factor is assigned a different weight. All assigned weights together is called a weighting scheme. These weights are variable, and the exact weighting scheme should be tailored to represent prevalent field conditions.

Six scenarios with individual weighting schemes were designed, to test the sensitivity of the objective function to changes in the multiplication factors. Table 1 shows an overview of the six scenarios and the corresponding weighting schemes.

Scenario 1 is a basic scenario, where the spraypath multiplication factor f_{SP} is equal to the work done in spraypaths compared to normal paths, where the distances in wet areas get a slightly higher weight than the distances in dry areas, where f_{UT} and f_{XT} are both equal to 1, adding a cost of 180 to the distance part of standard 180° turns, and where the headland movements have 80% of the influence of main field movements.

Scenario 2 is a scenario in which U-turns have a strong preference over X-turns, whilst in scenario 3 X-turns have a strong preference over U-turns. These scenarios were set up to represent personal preferences of farmers; Jacob van den Borne prefers to use mainly X-turns (personal communication, February 16, 2018), whereas Gert Oudijk strongly prefers U-turns (personal communication, February 9, 2018).

Table 1: The six weighting scheme scenarios set up to test the influence of the five different multiplication factors in the objective function.

	f_{SP}	f_W	f_{UT}	f_{XT}	f_{HL}
1. Basic	0.5	1.3	1	1	0.8
2. Go UT	0.5	1.3	0.5	6	0.8
3. Go XT	0.5	1.3	6	0.5	0.8
4. Dry	0.5	1	1	1	0.8
5. Wet	0.5	2	1	1	0.8
6. No HL	0.5	1.3	1	1	3

In scenarios 4 and 5 f_W is changed; scenario 4 is a dry scenario, where the wet areas are assumed to have dried and have no added influence compared to dry areas, whilst scenario 5 is a very wet scenario, in which driving through wet areas has a cost that is twice as high as the costs in dry areas. These scenarios were set up to represent different field conditions, depending on the

weather.

Scenario 6 is a scenario in which headland movements are far more important for the objective function than main field movements; in this scenario the headland movements cost 3 times as much as the main field movements. This scenario was set up to test the influence of f_{HL}, and to test whether a higher value of f_{HL} would move the focus of optimization more towards headland turns, and less on wet areas.

The six defined weighting scheme scenarios in Table 1 are tested on Test field 1 using seven defined movements and a test route. The movements are defined in Table 2. These movements are chosen to comprise the most common movements in agricultural fields. For each weighting scheme scenario the costs of these movements are calculated.

The defined test route was used to calculate the weightmeters of an entire route for each weighting scheme. The path order is shown in Figure 9, as the edge labels refer to the worked order. This defined path order generates a route starting in the depot, working the most upper path (spraypath), the most center path (wet), and the lowest path first, with all U-turns in between. Then the route leads back up towards the spraypath through the paths it skipped at first, with all X-turns in between, finishing the work in the path between node 10 and 11, after which it leads back to the depot. Due to the small size of the test field there is no intermediate depot visit in this route.

Finally, using an exhaustive search route planning approach, the optimal route was calculated for each weighting scheme.

The parameters for the objective function, W_{empty}, W_{full}, W_{bunker}, C_d, WCM, and r, were based on inputs of farmers Gert Oudijk and Jacob van den Borne to be realistic with true values. The total weight W at the start of each movement is set to 8,000 kg.

Table 2: Seven common movements defined to compare the six weighting scheme scenarios. Node numbers (From/to) correspond to numbers in graph representation in Figure 9.

From/to	Represents
6 , 12	U-turn
6 , 10	X-turn, long
6 , 8	X-turn, short
1 , -1	Depot visit, long
13 , -1	Depot visit, short
2 , 3	Working a dry path
8 , 9	Working a wet path

Table 3: Input parameters for the objective function used on Test field 1 and Test field 2 (introduced in section 2.2.2). Parameters are based on data supplied by farmers.

	Test fields 1 & 2
W_{empty} [kg]	7,150
W_{full} [kg]	8,850
W_{bunker} [kg]	1,700
C_d [cm]	166,500
WCM [kg/cm]	- 0.0102
r [cm]	400

2.2 Route optimization algorithm

Finding the optimal route to work all paths in a field is close to impossible for a normally sized field, since this capacitated vehicle routing problem is an NP-hard problem (Bakhtiari et al., 2012). An exhaustive search method calculates the objective function for all possible path orders. The number of possible path orders is equal to $n!$, with n being the number of paths in a field.

Therefore, the second research question aimed to find an efficient optimizer for the objective function. A route optimization algorithm should be able to find a near-optimal route within a reasonable time, by searching possible path orders in an efficient way. Numerous different optimization algorithms have been applied to (C)VRP's in previous researches. Four of them were identified and compared, in order to find the one that best suits this implementation of the CVRP. These four are used often in previous researches or seemed promising. The four identified optimization algorithms are the ant colony optimization algorithm (e.g. Bell and McMullen (2004); Bakhtiari et al. (2012)), the Tabu search algorithm (e.g.Barbarosoglu and Ozgur (1999); Cordeau and Laporte (2005)), the Clarke-Wright savings algorithm (e.g. Altınel and Öncan (2005)), and the genetic algorithm (e.g. Baker and Ayechew (2003)). Table 4 gives an overview of the comparison.

This comparison was based on three points:

- *Scopus search results 'CVRP + name algorithm'*
  For this comparison, three searches were performed on scientific literature search engine Scopus. For each of the four chosen optimization algorithm, a search was performed, reading 'capacitated vehicle routing problem' followed by the full name of the optimization algorithm. These searches produced different counts of results, used as a measure for the implementability of the algorithm in the capacitated vehicle routing problem.

- *Performance in (C)VRP*
  Extensive literature gave an idea of the performance of the optimization algorithms in different researches on the (capacitated) vehicle routing problem. The Tabu search jumped out as best performing algorithm, owing to the comparison by Laporte et al. (2000), who performed benchmark tests on different algorithms for the VRP. They found the best results with the Tabu search algorithm. They also found that calculations using the Clarke-Wright algorithm were fast, but results were highly unstable.

- *Implementable in Python script*
  The third point compared on-line available packages and implementations of the different optimization algorithms in Python. The most implementations were found for the Clarke-Wright algorithm and the Tabu search algorithm. These implementations were often well documented, in contrast with the found genetic algorithm implementations, which were extensive and unclear.

Table 4: Comparison of four optimization algorithms interesting for this research; ant colony optimization (ACO), Tabu search algorithm (TSA), Clarke-Wright savings algorithm (CWSA), and genetic algorithms (GA). In the second and third comparison, the range goes from - - (very bad) to ++ (very good), with 0 as center (normal).

	ACO	TSA	CWSA	GA
Scopus search results 'CVRP + name algorithm'	97	103	36	168
Performance in (C)VRP	+	++	-	+
Implementable in Python script	+	++	++	0

From this comparison, the Tabu search algorithm was chosen as the most suitable optimization algorithm for this research. Tabu search starts with an initial solution, after which it generates similar candidates, called neighbors, and moves to the best candidate at every iteration. To avoid getting stuck in a local minimum, candidates that were recently tested are *tabu* for a number of iterations, and are stored in a tabu list. (Laporte et al., 2000)

Numerous Python implementations of the Tabu search heuristic are available on-line. One of these, by Panyam, was a direct python implementation of the Tabu search algorithm presented in the book 'Clever Algorithms: Nature-Inspired Programming Recipes', by Brownlee. This made the script easy to understand and implement in a Python script, and adapt to work with the script of the objective function.

2.2.1 Implementation

Figure 10 gives a schematic overview of the Tabu search algorithm as it was implemented in the Python script. The cost graph created from a field with the first Python script is the main input of this second script. Besides the cost graph, three meta parameters are essential to determine how the algorithm performs; the number of iterations, the number of candidates, and the maximum length of the tabu list. The main output is the least cost path order found, with corresponding route and weightmeters.

The Tabu search algorithm starts by creating an initial path order from the field paths in the graph. For this initial path order, the objective function calculates the route and the weightmeters. The resulting route and weightmeters, together with the path order, are stored as the overall best result. The path order is also stored in the tabu list.

For every iteration, a given number of candidate path orders is created. Every candidate within an iteration is based on the best candidate of the previous iteration, with the candidates of the first iteration based on the initial path order. New candidates are created with a stochastic 2-opt local
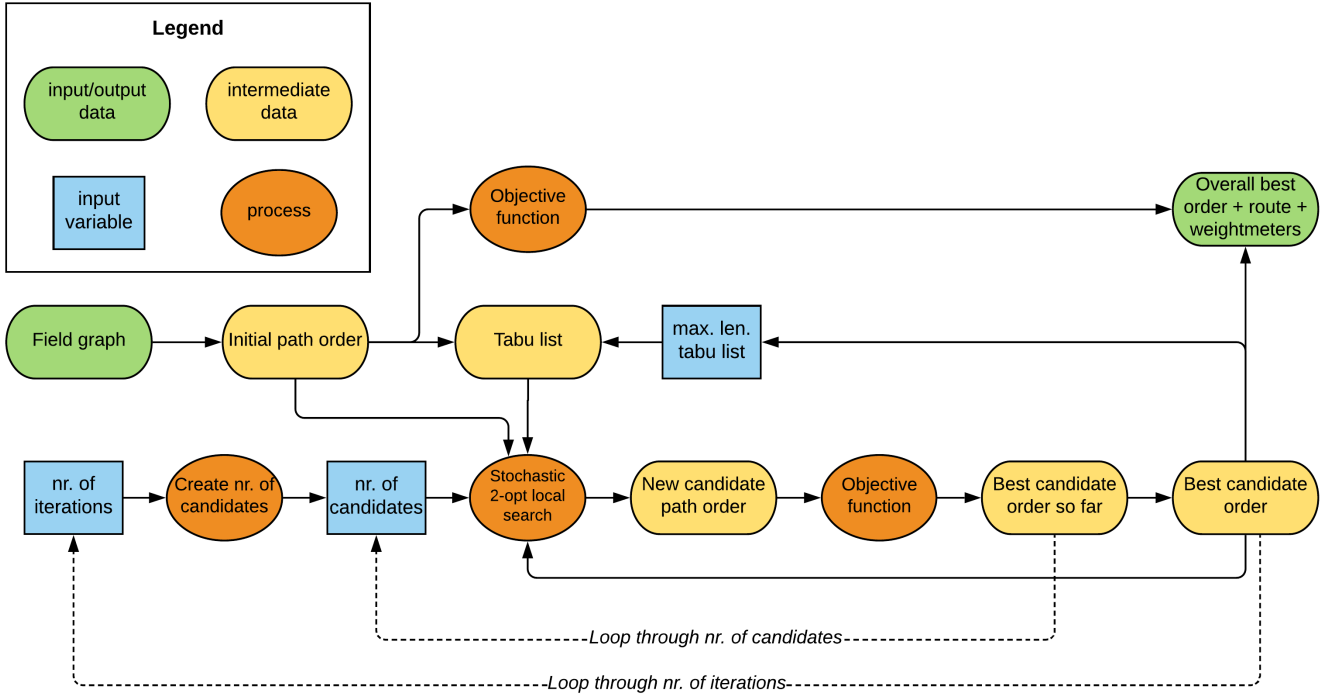
Figure 10: Schematic overview of the Tabu search algorithm as implemented in the Python script.

search process. This process takes two randomly chosen paths in a given path order, and reverses the order of the paths in between these two paths. Figure 11 gives a graphical presentation of this search process. Using this process, the Tabu search algorithm always searches in the neighborhood of the best solution of the previous iteration.
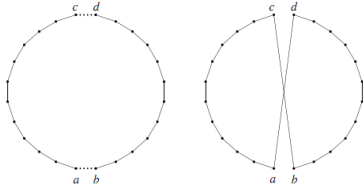

Figure 11: Graphical presentation of stochastic 2-opt local search process (Panyam).

For every candidate, the objective function is calculated, using the first Python script. The least cost path order within an iteration is stored in the tabu list. If the maximum length of the tabu list is reached, the oldest path order is removed from the list. The stochastic 2-opt local search process uses the tabu list as input; new candidate path orders are rejected if they are already present in the tabu list. This prevents the algorithm from getting stuck in a local minimum, though it is possible to return to the same minimum once the path order is removed from the list again.

The overall best path order, with corresponding route and weightmeters, is updated once a candidate has a lower cost than all previous candidates. This is the most important output of the algorithm. The algorithm also stores a list of weightmeters calculated for the least cost candidate for each iteration. This list gives insight in the improvement of the search algorithm per iteration.

2.2.2 Testing

To test the performance of the route optimization algorithm, the Python script was tested on five fields. The first one was Test field 1, the same test field as used in the testing of the objective function, as shown in Figure 9. The second field was Test field 2, a hypothetic but realistically sized field, based on the geometry of an existing field. It has 52 field paths with an average length of 237 meters. The graph created based on Test field 2 is shown in Figure 12. Besides these two generated test fields, the Python script was presented with three real-life fields, based on data and parameters supplied by farmers. More details on these three fields will follow in the next section.

Test field 1 is used to test the route optimization algorithm in comparison with an exhaustive search route planning. Owing to its small size, and the larger size of the other fields, this was the only field where exhaustive search route planning was an option, given the available computational power. The optimization algorithm takes three meta parameters as input to manage the search methods of the algorithm; the number of iterations, the number of candidates per iteration, and the maximum length of the tabu list. These three parameters where adjusted in six optimization scenarios indexed A to F, with increasing computational demands, to find the parameters for which the route optimization algorithm consistently finds

Table 5: The six optimization scenarios (Scn.) for the route optimization algorithm used on Test field 1, with different values for the number of iterations, number of candidates, and the maximum length of the tabu list.

Scn.	Iterations	Candidates	Tabu
A	50	2	5
B	50	5	5
C	50	5	10
D	50	10	10
E	50	25	10
F	100	25	10

the most optimal route for Test field 1. The six scenarios are shown in Table 5. The first scenario, scenario A, was set up as starting scenario, with very light computational demands. In scenarios B to F the parameters were incrementally tweaked. The resulting computing times of these route optimizations, as well as the costs for the found routes, were compared to the results of the exhaustive search approach. The computing times are calculated as the average time per run after 50 runs, for both the optimization algorithm and the exhaustive search route planning. The script had to be run multiple times due to the stochastic factor; multiple runs of the script gave insight in the stability of the results. The number 50 was chosen assuming it would give a good representation of performance of the algorithm on the long run.

The other four fields were used to test the power and limitations of the route optimization algorithm applied to normally sized fields. For the three meta parameters in the route optimization algorithm, twelve scenarios were defined, indexed 1 to 12, with increasing computational demands. The values defined per optimization scenario are shown in Table 6. The different optimization scenarios were defined from a practical perspective; the first scenario would produce a solution in a very short time, but the results are expected to have room for improvement, whilst the twelfth scenario would produce far better results at the expense of an unreasonable amount of time for its calculations. The intermediate scenarios were set up to test different combinations of meta parameters, in search for a balance between good results and short computing time.

Optimal routes were calculated 50 times for the four normally sized fields for every optimization scenario, to come to a sample size of 50 per scenario per field. This number was chosen with total computing time in mind; $n = 50$ was assumed to give a good representation of performance of the algorithm on the long run, without making the total computing time too high.

The results of the 50 calculations per optimization scenario per field were compared in tables and plots. Furthermore, the average computing times over the 50 computations per optimization scenario per field were stored and compared.

In all of these tests, the applied weighting scheme for the objective function was the Basic weighting scheme, as shown in Table 1. The performance of the optimizer is assumed not to be influenced by the weighting scheme of the objective function. The parameters for the objective function, W_{empty}, W_{full}, W_{bunker}, C_d, WCM, and r, were again based on the inputs of farmers Gert Oudijk and Jacob van den Borne to be realistic with true values, as shown in Tables 3 and 7.
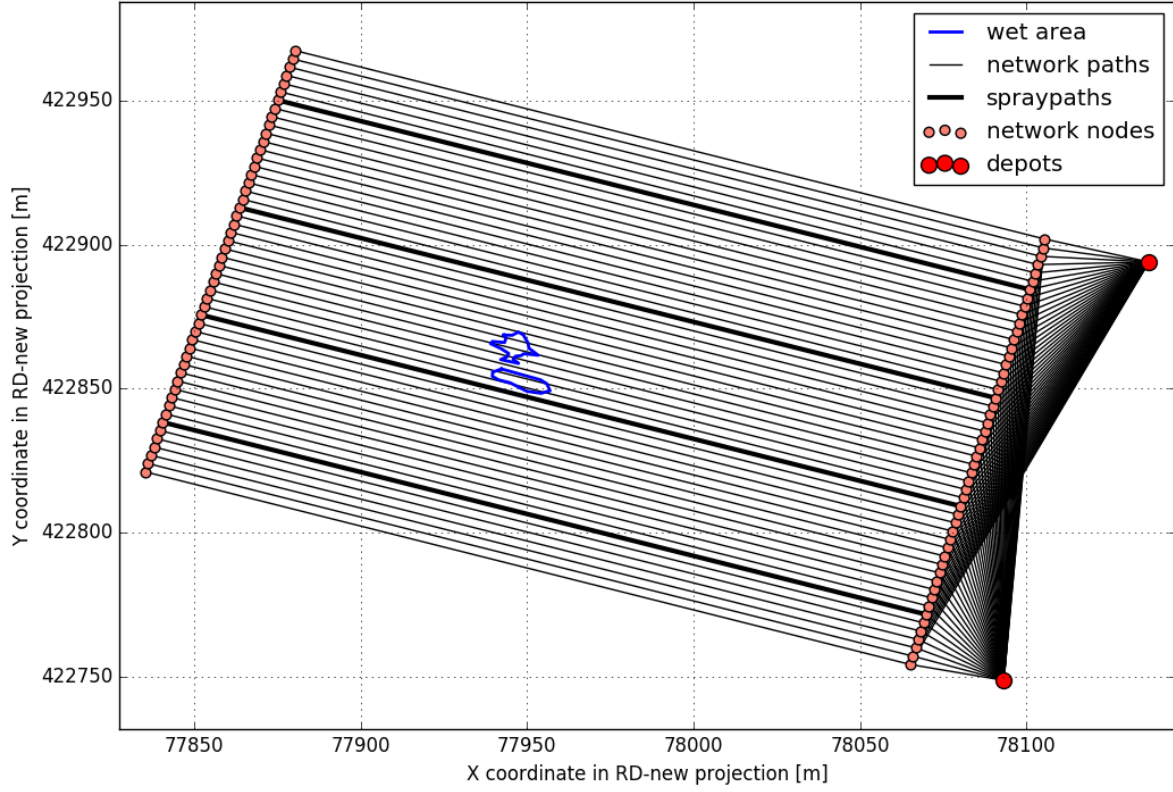
Figure 12: Graph representation of Test field 2, with the x- and y-axis giving coordinates of the nodes in RD-new projection [m].

Table 6: The twelve optimization scenarios (Scn.) for the route optimization algorithm used on fields Test field 2, Gert, Korsendonk, and Cools, with different values for the number of iterations, number of candidates, and the maximum length of the tabu list.

| Scn.	Iterations	Candidates	Tabu
1	50	20	5
2	50	20	15
3	50	20	50
4	200	20	50
5	200	100	50
6	1000	20	50
7	1000	100	5
8	1000	100	50
9	1000	100	250
10	5000	20	50
11	10000	100	50
12	50000	20	250

2.3 Test-cases

The algorithm defined in the previous research questions was applied to three real-life test-cases. These test-cases were based on input data received from farmers Jacob van den Borne and Gert Oudijk. Three fields were selected, and identified by the names field Gert, field Korsendonk, and field Cools. An overview of each of these fields is shown in Figure 13.

The data of the farmers consisted of point measurements with timestamps, measured during operations of planting potatoes. The timestamps made it possible to define the worked order of paths. Shapefiles of the paths in the main field, with spraypaths identified as such, were either given by the farmer or derived from the point measurements. This resulted in three files of lines of field paths, with information on spraypaths and worked order. Visual inspection of the fields with underlying Google satellite imagery revealed signs of variability in soil moisture. Figure 13 shows light and dark areas within the fields and in the surrounding areas of field Korsendonk (b) and field Cools (c), which is assumed to indicate variability in soil moisture. The satellite imagery also shows color changes in field Gert (a), but this is an artifact caused by different satellite image tiles. Therefore, and based on the information provided by the farmer, no wet areas were identified in Field Gert.

The differences in soil moisture in fields Korsendonk and Cools were supported by electrical conductivity measurement data from farmer Jacob van den Borne. These were measured with a DUALEM 21s sensor. Jacob van den Borne uses these electrical conductivity measurements as proxy measurements for soil moisture, since soil moisture is one of the main factors inducing differences in electrical conductivity within his fields. Therefore, these data were used to identify large wet areas within field Korsendonk and field Cools.

The exact locations of the depots were not given by the farmers, because the depots are flexible. The locations of a depot can vary a lot. Instead, depot locations were chosen based on satellite imagery. The locations are places where the field can be entered, or other places in the headlands that seemed ideal for a depot position because they are easily reachable from many field path ends.

The creation of the cost graphs of the test-case fields was in some cases not fully automatic. After running the script to create the first graph, representing the possible moves within a field, some edges had to be removed manually because they represented unrealistic movements.
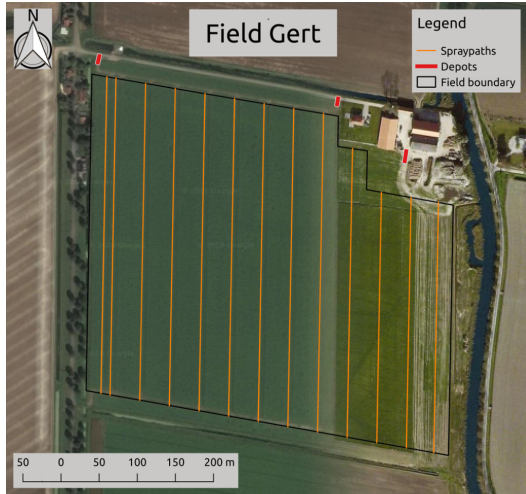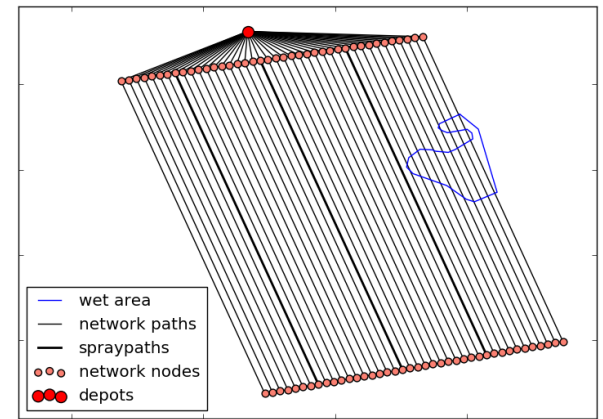
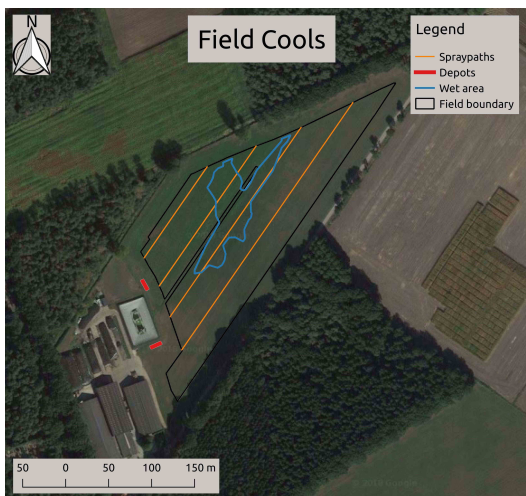(a) Field Gert, based on data from farmer Gert Oud-
ijk.
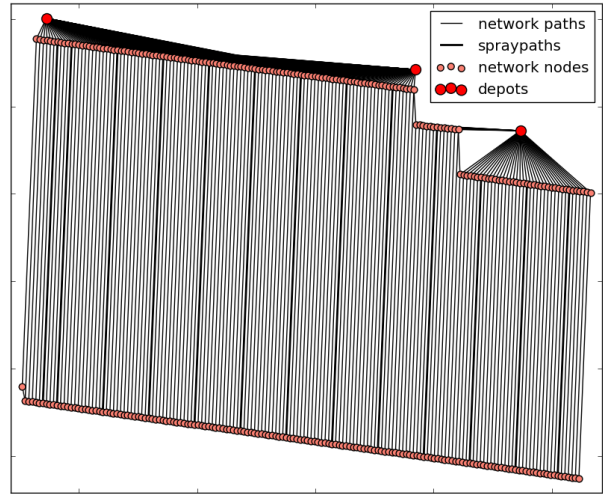
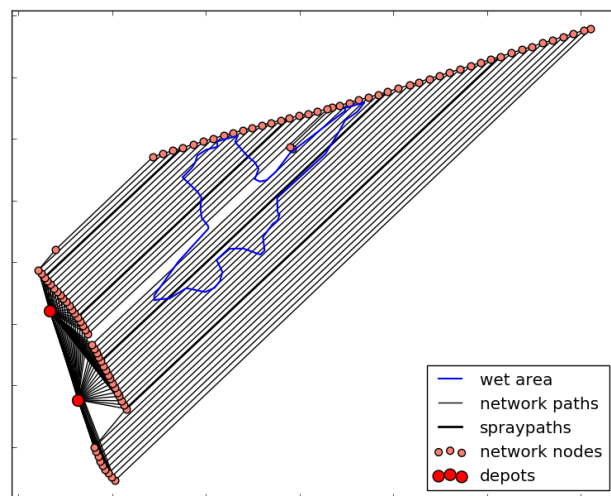(b) Representation of the graph based on Field Gert.
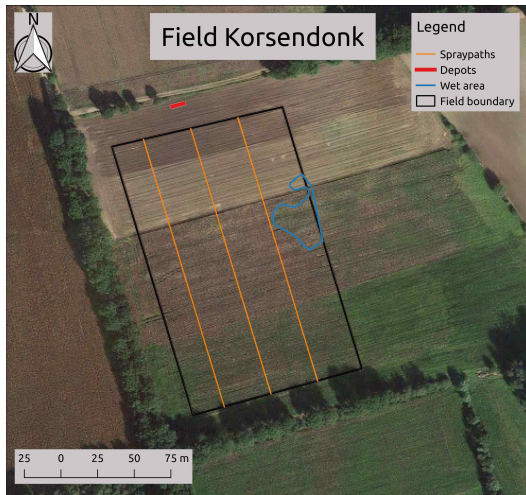
(c) Field Korsendonk, based on data from farmer
Jacob
van de Borne

(d) Representation of the graph based on Field Korsendonk.

(e) Field Cools, based on data from farmer Jacob van
den Borne

(f) Representation of the graph based on Field Cools.

Figure 13: Maps of main field boundaries, spraypaths, depots, and wet areas in the three fields
used as test cases, with underlying Google satellite imagery. The normal field paths are left out of
these images to give a clearer overview.

Field Gert   Figure 13a shows that Field Gert is close to rectangular, but contains a large gap where the farmhouse is positioned. Two depots are positioned where the field can be entered from the road, and one where the field can be entered from the farmhouse, bringing the total number of depots to three. Figure 13b shows that not all path ends on the northern side of the field are connected directly to all depots. The path ends of the shorter paths on the right side of the field are only directly connected to the most right depot, while all path ends on the longer field paths are only directly connected to the center and left depot. Field Gert contains no wet area, as explained before. Field Gert is the largest test case field, with 159 field paths.

Field Korsendonk   Figure 13c shows that Field Korsendonk is simply rectangular. Therefore, the graph based on Field Korsendonk, as shown in Figure 13d, is generated automatically, using the same Python script as applied to the two hypothetical test fields. The depot is positioned in the center of the headland on the side of the road, and all path ends on the same side of the field are directly connected to the depot, representing straight moves between the depot and the path ends.

The wettest area within Field Korsendonk was measured to be on the right side of the field, close to half way the field paths, covering the ten most right field paths. The field is the smallest true test field, with only 40 field paths.

Field Cools   Figure 13e shows that Field Cools departs most from a rectangular shape. Still the field was treated the same as the other fields, with only three exceptions; the three shortest field paths cannot be visited from the depots in one straight movement, and vice versa. This was mainly due to an impassable stretch in the field, creating two short paths.

These two shortest field paths are positioned in the center of the field. Because these field paths do not cover the entire main field they can only be reached from one side of the field. The edges representing movements between these two field paths and the depots were removed manually from the first graph, along with edges connecting their path ends with other path ends on the depot side of the field.

The third exception was the field path on the North-Western side of the field. The edges representing straight movements between this field path and the depots were replaced by movements that first visit the neighboring field path end. A straight movement between the field path end and the depots would intersect with neighboring field paths, which is unrealistic.

The wet area in Field Cools is a large area in the center of the field. Two depots were positioned in the headland on the side of the farmhouse, at places that seemed logical. The field is relatively small, with 46 field paths in total.

Besides these field data, the farmers were asked to supply data on working unit weights, distance capacity, and turning radius of the working units used during operations of planting potatoes. These data and the derived parameters are shown in Table 7.

Both farmers supplied W_{empty} and W_{bunker}, from which W_{full} was calculated. For field Gert, the distance capacity was given as four paths. To translate this to centimeters, the distances of the four longest paths in field Gert were summed and rounded up to meter level, which gave a value of 1,665 m. From these values, WCM [kg/cm] was calculated using Equation 5. For the fields Cools and Korsendonk, weight of planted potatoes per hectare [kg/ha] was given. For both fields the lengths of all the paths in the main fields were summed, and divided by the total area of the fields, giving an average value of distance of paths per hectare [cm/ha]. Dividing the weight of potatoes planted per hectare by the distance of paths per hectare gave the WCM for fields Cools and Korsendonk. Equation 5 was used to calculate C_d from the WCM, W_{empty}, and W_{full}. C_d was then again rounded up to meter level, resulting in a value of 2,018 m for fields Korsendonk and Cools. Turning radius r was provided by both farmers.

Table 7: Input parameters per field for the test-cases supplied by the farmers or derived from data supplied by the farmers.

	Gert	Cools + Korsendonk
W_{empty} [kg]	7,150	14,000
W_{full} [kg]	8,850	16,000
W_{bunker} [kg]	1,700	2,000
C_d [m]	1,665	2,018
WCM [kg/cm]	- 0.0102	- 0.0099
r [cm]	550	400

Using these files and parameters as input, the Python scripts with the objective function and the Tabu search algorithm were tested to generate near-optimal routes through the given paths. The values of the objective function of the routes found by the algorithm were compared to those of the route based on the path orders chosen by the farmers.

3 Results

In this chapter the results are shown and explained. The results are presented per research question, in the same order as the methods. These results are discussed in the next chapter.

3.1 Definition of an optimal route

An optimal route is obtained by minimizing the objective function J (Equation 7). This objective function takes five multiplication factors as input, together forming a weighting scheme. The influence of different weighting schemes on the costs of different movements and on a test route was tested in Test field 1. The influence of the weighting schemes was also tested using an exhaustive search method for finding the optimal route.

Table 8 shows the first results, on the influence of different weighting schemes on different common movements and a given test route. The resulting costs are given in weightmeters for the seven tested movements and the total test route per defined weighting scheme scenario.

The table shows that the short movement towards the depot, between nodes 13 and -1, is the move with the lowest costs in all scenarios. A short X-turn movement costs more than a longer X-turn movement, in all scenarios, and more than an even longer U-turn in all scenarios but scenario 3. In scenarios 1 to 5 the headland movements have costs lower than the main field or working movements. The total costs of the test route seems to be very constant, and only changes, within the given precision, when the influence of wet areas is changed (scenarios 4 and 5). This total cost is lowest in the dry scenario, and highest in the wet scenario.

Table 8: Costs in weightmeters for seven tested common movements, per weighting scheme scenario, for $W = 8,000kg$ at the start of each movement. The costs are shown in the unit $10^4 m * kg$. The pairs of nodes (From/To) of these movements correspond to the node numbers in Figure 14. See Table 1 for details on the weighting scheme scenarios.

From/To	Movement	1.Basic	2.Go UT	3.Go XT	4.Dry	5.Wet	6.No HL
6, 12	U-turn	9.4	9.3	15.6	9.8	9.8	36.9
6, 10	X-turn, long	10.5	16.2	9.9	10.5	10.5	39.3
6, 8	X-turn, short	12.4	18.2	11.8	12.4	12.4	46.5
1, -1	Depot, long	18.5	18.3	21.1	18.5	18.5	69.5
13, -1	Depot, short	7.1	6.9	9.0	7.09	7.1	26.6
2, 3	Work, dry	35.1	35.1	35.1	35.1	35.1	35.1
8, 9	Work, wet	40.3	40.3	40.3	35.1	52.6	40.3
	Test route	260	260	260	248	286	260

Table 9 shows the path orders representing the optimal routes found using an exhaustive search method for each of the six investigated weighting scheme scenarios. These path orders are also shown in the graph representation in Figure 14. The path order resulting in the optimal routes was identical for scenarios 1, 2, 3, 5, and 6, and is shown in Figure 14a. The optimal path order was only different for the weighting scheme of the dry scenario, scenario 4. That path order is shown in Figure 14b. In both path orders, the spraypath would be worked first. Figure 14a. shows that in most scenarios the field paths through the wet area (with nodes 6, 8, and 10) were selected to be worked last. Note that the sequence of paths crossing wet spots was ordered according to distance traveled through wet area. The field path with node 8, with the longest distance through the wet area, would be worked last in all weighting scheme scenarios.

In the dry scenario, Figure 14b, the path order resulting in the optimal route was a path order with less neighboring field paths worked consecutively. In Figure 14a, the third and fourth path in the path order are neighboring paths, as well as the sixth and seventh. In Figure 14b, the fifth and sixth paths are the only neighboring paths that would be worked consecutively. In the dry scenario, the paths with nodes 12 and 8 would be worked first and last, respectively, the same as in the other scenarios. The optimal order of the field paths with nodes 4, 0, and 2 was also equal in all scenarios. The field paths with nodes 6 and 10 would however be worked second and third in the dry scenario, instead of sixth and seventh in the five other scenarios, respectively.

Table 9: The path orders defined as optimal through Test field 1 per weighting scheme scenario, found using an exhaustive search method, and the weightmeters calculated for the total route. The numbers define a node number of the path to be worked, and correspond to the node numbers in Figure 14.

Scn.	Optimal path order	weightmeters [m*kg]
1. Basic	[12, 4, 0, 2, 10, 6, 8]	2594618
2. Go UT	[12, 4, 0, 2, 10, 6, 8]	2594653
3. Go XT	[12, 4, 0, 2, 10, 6, 8]	2594634
4. Dry	[12, 6, 10, 4, 0, 2, 8]	2483833
5. Wet	[12, 4, 0, 2, 10, 6, 8]	2852955
6. No HL	[12, 4, 0, 2, 10, 6, 8]	2594954
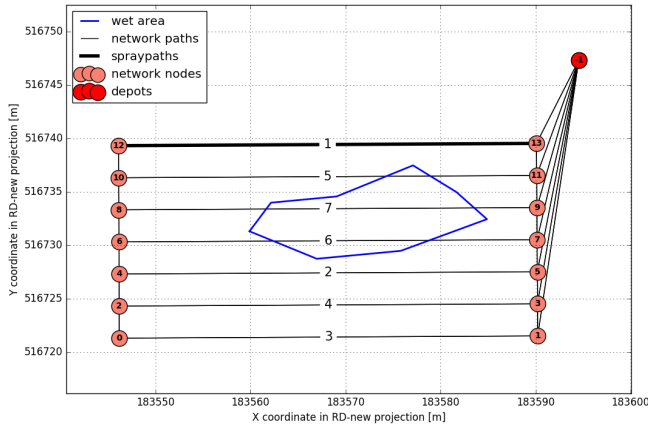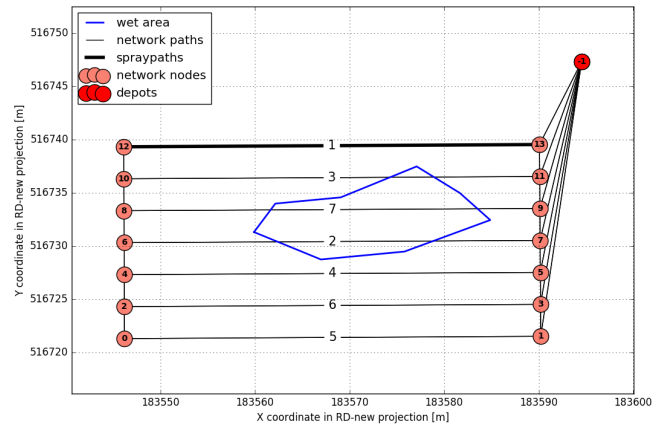
(a)   (b)

Figure 14: Graph of Test field 1, with field edges labeled according to optimal path order for weighting scheme scenarios 1,2,3,5, and 6 (a), and for scenario 4 (b), as depicted in Table 9.

3.2 Route optimization algorithm

The developed route optimization algorithm, based on a Tabu search algorithm, was tested on five different fields. Two hypothetical test fields (Test field 1 and Test field 2) and three fields based on input data from farmers (Fields Gert, Korsendonk, and Cools).

3.2.1 Optimizer versus exhaustive search

For Test field 1 the computation time as well as the results of the route optimization algorithm were compared with an exhaustive search route planning. Starting with a computational light optimization scenario the three meta parameters for the optimization algorithm were incrementally tweaked until the route optimization algorithm consistently produced the same optimal route as the exhaustive search method. This resulted in six optimization scenarios indexed A to F.

The average computing times and weightmeters are shown in Table 10 per optimization scenario. An impression of the distribution of the resulting weightmeters of the 50 runs are shown in Figure 15. Scenarios D, E, and F consistently found the optimal route for Test field 1, with weightmeters equal to the route found by the exhaustive search method. The average computing times for these three scenarios lied within a wide range, between 4.64 and 47.24 ms. The three scenarios with lower computing times (A, B, and C) showed higher costs in weightmeters in several of the 50 runs. The average computing time of the exhaustive search route planning was 65.646 ms, which is larger than all average computing times from the route optimization algorithm. Scenario D is the fastest optimization scenario that successfully found the optimal route 50 times, with a computing time of only 15.2 % of the computing time of the exhaustive search approach.

Table 10: Average computing times and average weightmeters [m*kg] for route optimization within Test field 1, for six optimization algorithm scenarios and exhaustive search route planning. Average computing times given in total (T [ms]) and compared to the exhaustive search(T [%]). Times and weightmeters averaged over 50 computations.

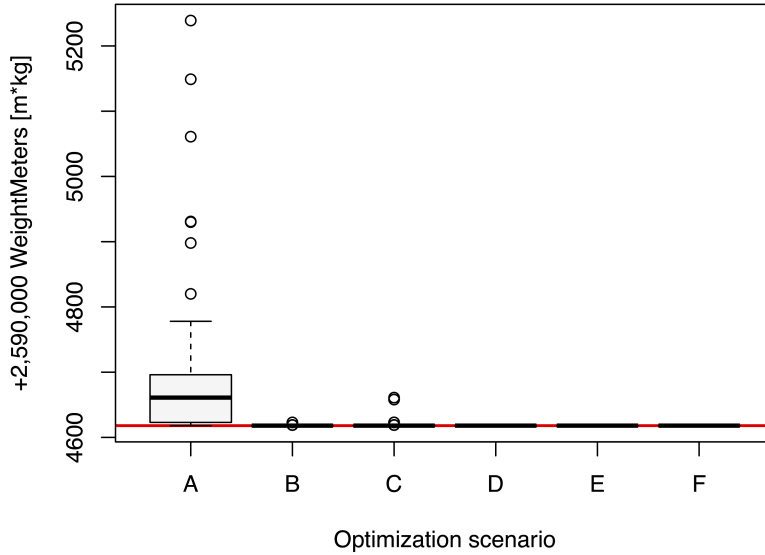| Scn.	Iterations	Candidates	Tabu	T [ms]	T [%]	weightmeters
A	50	2	5	2.057	3.13	2594714.3
B	50	5	5	4.607	7.02	2594620.2
C	50	5	10	4.641	7.07	2594618.4
D	50	10	10	9.971	15.2	2594618.0
E	50	25	10	24.582	37.5	2594618.0
F	100	25	10	47.235	72.0	2594618.0
Exhaustive search				65.646	100	2594618.0

Figure 15: Comparison of exhaustive search route planning and route optimization algorithm. Every boxplot represents an optimization scenario, with letters on the x-axis corresponding to Table 10. The y-axis represents the route costs in weightmeters. The red line represents the costs found by exhaustive route planning.

3.2.2 Optimization scenarios for normally sized fields

The four other fields were used to further test the influence of the three meta parameters, using twelve new optimization scenarios. For every optimization scenario, the route optimization algorithm was run 50 times. Figure 16 illustrates the distribution of the 50 results per optimization scenario. The average computing times as well as the average weightmeters are given in Table 11.

Overall, the resulting distributions are rather wide, with the exception of Test field 2. In the three real fields scenario 12 resulted in the most narrow distributions of costs. Test field 2 was an exception; in this field scenario 10 was the only scenario were results show no indication of outliers. In all four fields, scenario 12 resulted in the lowest average costs in weightmeters, and in the highest average computing times (Table 11).

Scenarios 1, 2, and 3 as well as 7, 8, and 9 were set up to test the influence of the length of the tabu list; in these two groups of scenarios the number of iterations and candidates was constant, while the length of the tabu list changed. The resulting distributions within these two groups were very similar for all tested fields, on average as well as in the distribution. A longer tabu list did not have a large influence on the results.

Scenarios 4 and 5 as well as 6 and 8 were set up to test the influence of the number of candidates; in these two groups of scenarios the number of iterations and length of the tabu list were constant,

while the number of candidates changed. The resulting distributions show that for fields Test field 2, Korsendonk, and Cools the optimization algorithm performed better with 20 candidates compared to 100 candidates. Note that in these fields, the results found with optimization scenario 10 were also better than the results found with scenario 11, whilst scenario 11 had more candidates and more iterations. Field Gert is the only field where the results improved for all these three described cases. Table 11 shows that field Gert has more than three times the number of field paths of the other three fields.

Scenarios 3, 4, 6, and 10 as well as 5, 8, and 11 were set up to test the influence of the number of iterations; in these two groups of scenarios the number of candidates and length of the tabu list were constant, while the number of iterations changed. The resulting distributions show that within the first group of scenarios a higher number of iterations resulted in lower costs on average for every field (see Table 11). However, for scenarios 5, 8, and 11 the results only improved noticeably for field Gert. In the other three fields, the results of these three scenarios were very similar.

Note from Table 11 that computing times were higher when number of iterations multiplied with number of candidates increased. In scenarios where number of iterations multiplied with number of candidates was equal (scenarios 1 to 3, scenarios 5 and 6, scenarios 7 to 10, and scenarios 11 and 12), the resulting average computing times within one field were in most cases very similar. Furthermore, Table 11 shows that for all scenarios the average computing time increased with an increase of number of paths. Calculations for field Korsendonk (40 field paths) resulted in the shortest computing times, whilst calculations for field Gert (159 field paths) resulted in the longest computing times per scenario.

(a) Test field 2

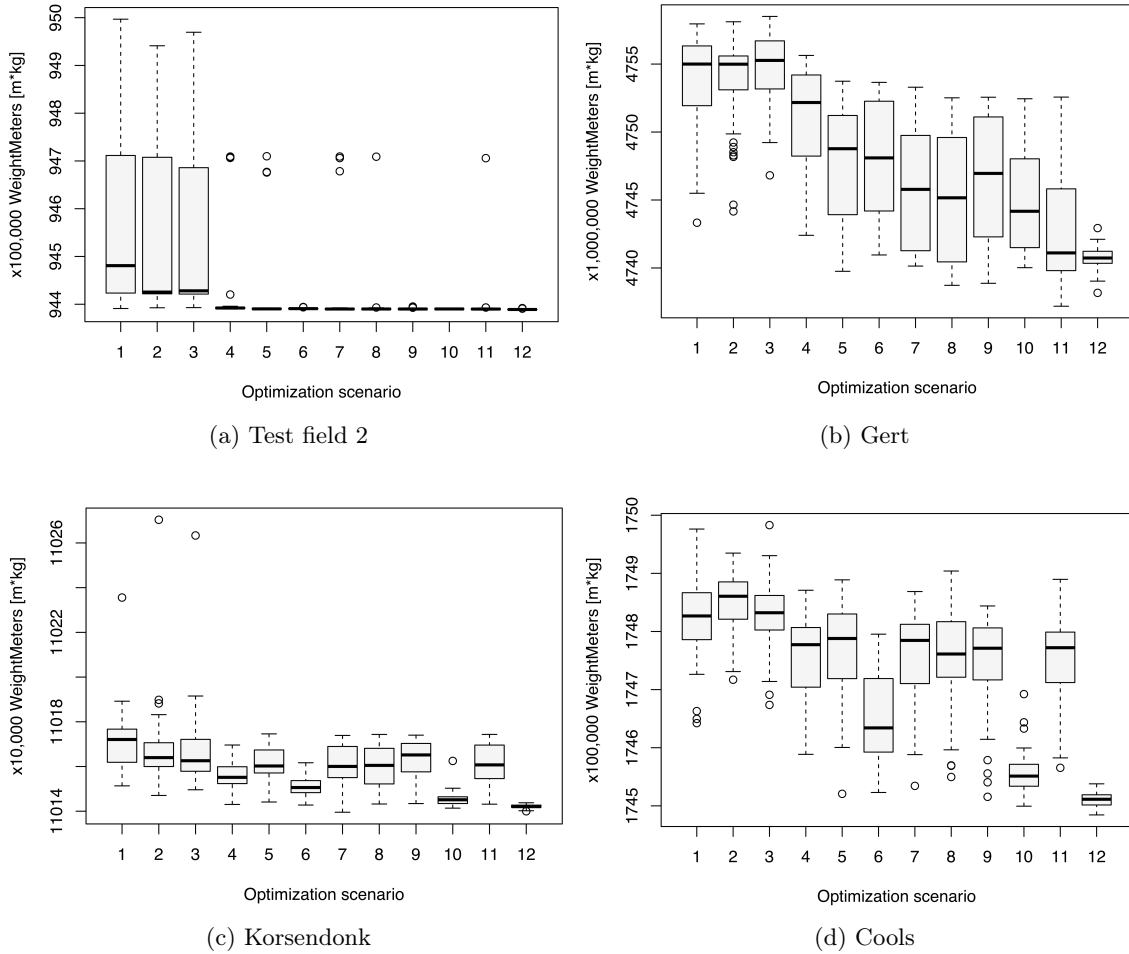(b) Gert

(c) Korsendonk

(d) Cools

Figure 16: Boxplots illustrating the distribution of the costs in weightmeters of 50 route optimizations per eight optimization scenarios, per field. The scenarios correspond to Table 11.

Table 11: Average computing time (T [s]) and costs in weightmeters (WM [10^4 m*kg]) over 50 runs of the route optimization algorithm, for twelve optimization scenarios over 4 fields. Nr. of paths shows the number of field paths per field. Costs of route chosen by farmer are displayed for the three test case fields. It. × Can. shows the multiplication of nr. of iterations and nr. of candidates per optimization scenario.

| | | Field = | | | Test field 2 | | Gert | | Korsendonk | | Cools | |
| | | nr. of paths = | | | 52 | | 159 | | 40 | | 46 | |
Scn.	It.	Can.	It. × Can.	Tabu	T	WM	T	WM	T	WM	T	WM
1	50	20	1,000	5	0.131	9455.82	0.541	47539.09	0.0843	11017.04	0.131	17482.41
2	50	20	1,000	15	0.129	9451.70	0.587	47538.63	0.0845	11016.76	0.143	17485.05
3	50	20	1,000	50	0.130	9450.84	0.536	47546.50	0.0850	11016.64	0.109	17482.60
4	200	20	4,000	50	0.522	9441.79	2.42	47508.13	0.342	11015.60	0.450	17475.29
5	200	100	20,000	50	2.55	9440.81	10.5	47475.71	1.68	11016.14	2.35	17477.07
6	1,000	20	20,000	50	2.60	9439.09	11.7	47477.91	1.75	11015.10	2.41	17465.08
7	1,000	100	100,000	5	13.4	9439.03	56.1	47458.16	8.56	11016.14	10.8	17474.85
8	1,000	100	100,000	50	12.7	9440.85	55.1	47449.65	9.85	11016.09	12.2	17475.63
9	1,000	100	100,000	250	14.6	9439.65	61.0	47467.80	8.41	11016.32	10.7	17475.74
10	5,000	20	100,000	50	13.7	9439.03	60.6	47448.63	8.91	11014.55	11.0	17455.76
11	10,000	100	1,000,000	50	137	9439.63	561	47429.50	86.4	11016.11	107	17474.74
12	50,000	20	1,000,000	250	132	9438.91	730	47407.42	90.1	11014.21	110	17451.09
		Farmers route						47716.15		11057.90		17593.75

27

3.3 Test-cases

Data of farmers Gert Oudijk and Jacob van den Borne measured during operations of planting potatoes were used to compare routes chosen by farmers, based on personal experience and knowledge, with routes calculated by the route optimization algorithm. The results of these comparisons are presented in this section.

Table 11 shows the costs in weightmeters for the least cost routes computed by the route optimization algorithm, per optimization scenario, averaged over 50 runs of the algorithm. The bottom row lists the costs in weightmeters for the routes based on the path orders chosen by the farmers. Figure 17 shows a graphical comparison between the costs calculated with 50 runs of the algorithm, and the costs calculated for the farmers routes. Both the table and the figure show a large difference between the costs from the optimization algorithm and the costs of the farmers routes. The costs of the routes based on the input of the farmers were consistently higher.

In Figure 19 the graphs of the three fields are shown, with colors depicting when a path is (suggested to be) worked between two depot visits. Figure 18 shows the legend corresponding to these graph representations. For every field the graph is mapped twice; once based on the path order as chosen by the farmer (left), and once based on the least cost route found per field during all 12x50 runs of the optimization algorithm (right).

In all optimized figures it stands out that spraypaths are worked soon after depot visits, shown by the green colors of the thicker field edges. The spraypaths are thus worked with a relatively high weight in the optimized routes. This is the best observed difference with the routes chosen by the farmers. In the wet areas in fields Korsendonk and Cools no consistent change is observed; in field Korsendonk the paths through the wet area are worked sooner after a depot visit, with a higher weight, whereas in field Korsendonk the paths through the wet area are worked later after a depot visit, thus with a lower weight. In the least cost route found through Test field 2 (not shown), the paths through the wet areas are also selected to be worked just before depot visits, with a relatively low weight.

Though it is not shown in these figures, it is important to know that the three path orders chosen by the farmers are regularly ordered, working from one side of the field to the other. For both farmers, regularly ordered routes were preferred due to ease of planning, and because they did not keep the weight of the working unit in mind during route planning. Farmer Jacob van den Borne had a personal preference for X-turns (personal communication, February 16, 2018). Farmer Gert Oudijk mentioned that he believes that the impact of the weight of the bunker on soil compaction is negligible (personal communication, February 9, 2018). All three path orders computed by the route optimization algorithm are ordered less regularly, suggesting to work the field paths in a more scattered order.

The largest improvement in weightmeters after optimization is found in field Cools.

(a) Field Gert

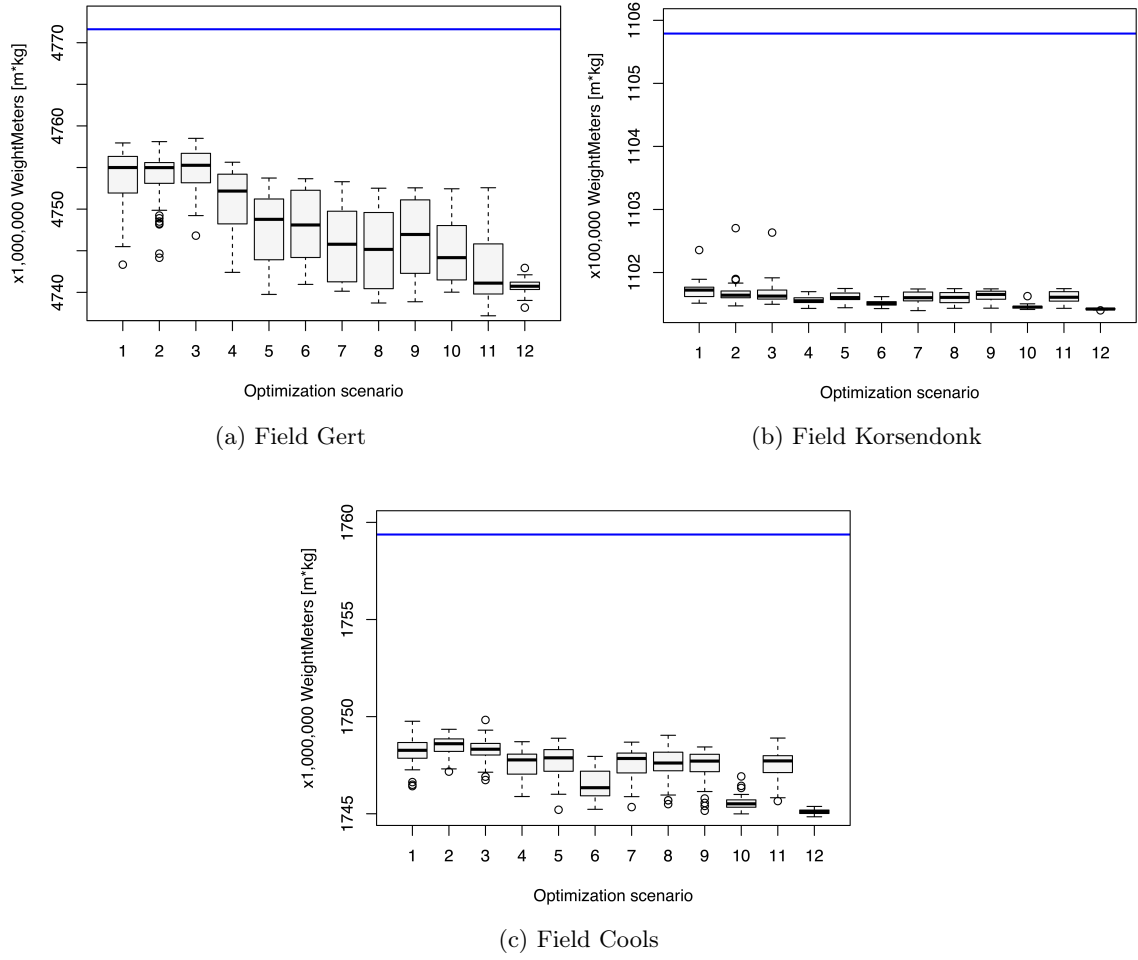(b) Field Korsendonk

(c) Field Cools

Figure 17: Boxplots of weightmeters calculated using the optimization scenarios per field, as shown in Figure 16, compared to the weightmeters calculated for the routes chosen by the farmers. The blue horizontal line represents the costs of the farmers routes.
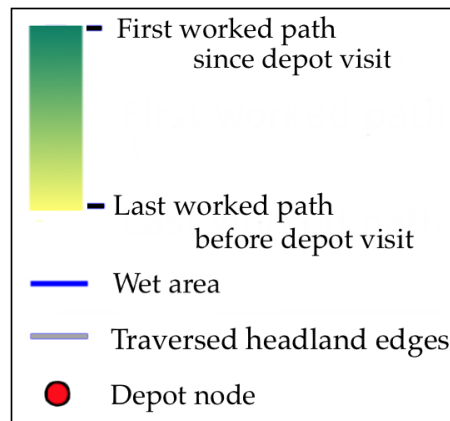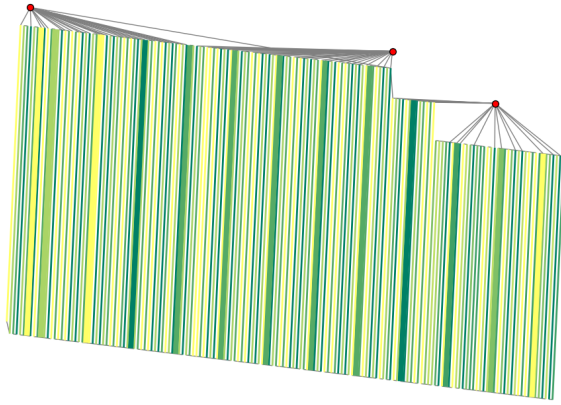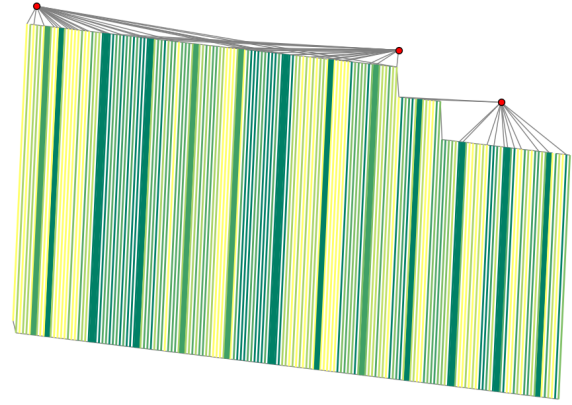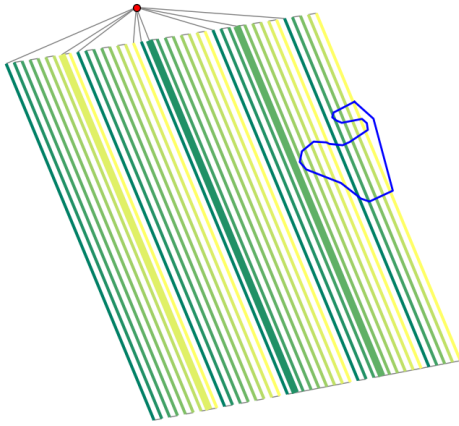

Figure 18: Legend for Figure 19. Edges are colored for each part of a route between two depot visits. Thicker edges represent spraypaths. Field nodes are not depicted.
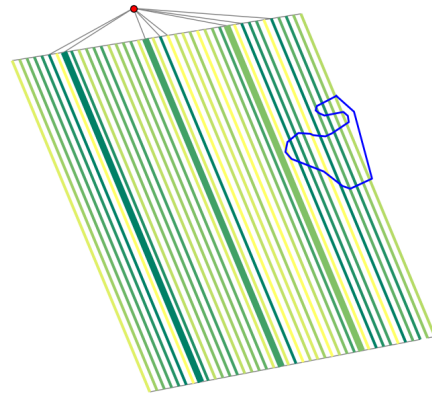
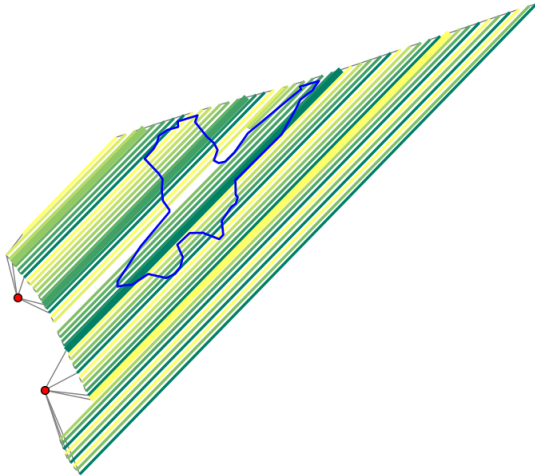(a) Field Gert, chosen by farmer,
weightmeters = 47.41 * 10^7 m*kg.

(b) Field Gert, optimized,
weightmeters = 47.39 * 10^7 m*kg.
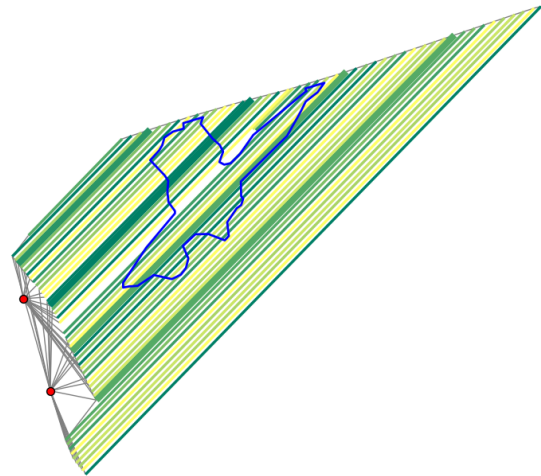
(c) Field Korsendonk, chosen by farmer,
weightmeters = 11.06 * 10^7 m*kg.

(d) Field Korsendonk, optimized,
weightmeters = 11.01 * 10^7 m*kg.

(e) Field Cools, chosen by farmer,
weightmeters = 17.59 * 10^7 m*kg.

(f) Field Cools, optimized,
weightmeters = 17.45 * 10^7 m*kg.

Figure 19: Maps with path orders per test case field. Left (a, c, e) path orders chosen by farmers, right (b,d,f) path orders computed by route optimization algorithm. For each part of a route between two depot visits the color gradient is reset; a greener color thus means a higher weight of the working unit. Numbers indicate total path order.

4 Discussion

At the start of this research, the following problem was defined; there is need for routes for agricultural field operations that minimize soil compaction by dealing with the two most important compaction factors, heavy machinery and soil moisture content. This lead to the objective to determine an optimal route for capacitated agricultural operations over predefined field tracks given local differences in susceptibility to compaction (e.g. wet spots). This objective was reached by answering the following research questions:

- What defines an optimal route for capacitated operations under spatially varying field circumstances?

- What optimization algorithm is best suited for finding such routes?

- Do test-case results of selected fields show an improvement over conventional routing?

This chapter will discuss the methods and results per research question.

4.1 Definition of an optimal route

An optimal route is defined as the route with minimal induced soil compaction. The current study proposed a weighted sum objective function to calculate the costs of a route through an agricultural field in weightmeters [m*kg], defining the optimality of the route with regard to soil compaction. Results show that the exact costs depend on the weighting scheme of the multiplication factors.

Tests on the influence of common movements show that an X-turn between two neighboring field paths has a higher costs than an X-turn between two field paths further apart (Table 9). This is a logical result when looking back at Equation 3. In this equation, a larger distance of an X-turn movement parallel to the main field border, d_{XT}, results in a lower cost. Sabelhaus et al. (2013) found an identical result for omega turns; with a larger distance between consecutive field paths the length of the turning path decreased.

A change in f_{UT} and f_{XT}, in weighting scheme scenarios 2 and 3, resulted in quite large differences in costs for the headland movements. However, in the small test field where these tests were conducted the optimal route did not change, as shown in Figure 14. This is most likely due to the relatively small distances traveled in headland movements, compared to main field movements, and the large wet area in the main field. The influence of the large wet area overshadows the influence of costs of different turns. The costs for headland movements are, apart from scenario 6, much lower than the costs for working a field path, either wet or dry. This again demonstrates the relatively small impact of costs for different headland movements. This small test field has very short field paths; in a normally sized field the field paths are longer, leading to an even smaller influence of headland costs.

This study focuses mainly on decreasing soil compaction in the main field, as this is the most important part of a field with the highest yields. The wet areas have a particular importance. In this light, the routes defined as optimal by the objective function are indeed desirable. They minimize the weight in the wet area and minimize the number of short X-turns. Small changes of the wet multiplication factor had a large influence on the resulting costs, as well as on the optimal route within the small test field (see Table 8). If however a farmer would like to focus on headland movements, to decrease soil compaction in the most trafficked areas, the headland multiplication factor f_{HL} should be set considerably higher.

A downside to the used method is that it assumes simple rectangular fields. An input field should have headlands on two sides of the main field, no more and no less, and the depots should be reachable in a straight line from every path end on the same side of the field. If one of these assumptions is not met, the graph based on the field should be manually modified to resemble plausible movements. This was for instance necessary for the fields Gert and Cools in the test cases (section 2.3).

The choice when to visit a depot is of major impact for the costs of a route. This is however based on a very simple condition; whether or not the next field path in the path order can be worked entirely, before reaching bunker capacity. This might lead to a path being worked after which it has to visit a depot, whilst the depot is positioned on the other side of the main field, close to where the working unit was before working the path. The total costs for a route might in such cases be lower if a depot is visited first, before working the path, before the currently set

condition is met. However, incorporating this choice whether or not to visit a depot after every worked path was unfortunately unfeasible, because the number of possible routes would increase drastically, leading to a too complex problem.

In the current study, wet areas are discrete data; a part of a field is either wet or not (section 2.1.5). This is however a large simplification of the true world. The wetness of a field cannot be captured in two values, it is rather continuous data. Furthermore, the susceptibility to soil compaction depends on more soil properties than just soil moisture content, e.g. clay content and soil organic material (Hamza and Anderson, 2005). The choice to only incorporate discrete wet areas is made to simplify the input needed from farmers, and because soil moisture content is the most significant soil property with regard to soil compaction (Hamza and Anderson, 2005). It is important to keep these simplifications in mind when inspecting the results.

4.2 Route optimization algorithm

To approach the overall optimal route, without exhaustively calculating optimality of all possible path orders, an optimization algorithm is introduced. The Tabu search algorithm was chosen as optimization algorithm, based mainly on previous successful researches and ease of implementation in a Python script (section 2.2). The optimization algorithm was successfully implemented with the objective function.

On a small test field, the optimization algorithm was compared with an exhaustive search approach. Six optimization scenarios were set up, with increasing computational demands. Results are shown in Table 10. The exhaustive search approach found the optimal route 50 times, with an average computing time of 65.649 ms. Running the optimization algorithm 50 times resulted in average computing times between 2.057 and 47.235 ms. The lightest optimization scenario that found the same result as the exhaustive search in all 50 runs of the algorithm, scenario D, did so in an average time of 9.971 ms. On this small test field, the optimization algorithm consistently found the optimal route in only 15.2% of the computing time of an exhaustive search approach.

The optimization algorithm takes three parameters as input to manage the search methods. The influence of these parameters was tested on four larger fields, using 50 runs of the optimization algorithm for 12 optimization scenarios. Results are shown in section 3.2.2.

In three out of four fields, the distributions of the 50 results are rather wide (Figure 16). The most demanding optimization scenario, scenario 12, resulted in the narrowest distribution of the results for these fields. For one field, the narrowest distribution was found in scenario 10. In all fields the average resulting costs in weightmeters were lowest and the average computing times were highest in the most demanding optimization scenario, with 50,000 iterations and 20 candidates (Table 11). However, these settings resulted in computing times from 90 up to 730 seconds, close to 12 minutes, on average per run. And still the distributions resulting from this scenario showed much overlap with distributions of scenarios with lower computing demands, which proves that in numerous cases a scenario with lower computing demands found a better route as result. In other words, although optimization scenario 12 results in the lowest weightmeters on average, a combination of parameters that runs with much lower computing times might as well return a better route.

The influence of the length of the tabu list on the results was unnoticed, both the costs and the computing times. The number of candidates and iterations had far more influence. Surprisingly, in the three smallest fields out of four tested fields, optimization scenarios with 20 candidates returned better results than optimization scenarios with the same number of iterations but with 100 candidates (scenarios 4 and 5, and 6 and 8, in Figure 16). In the same three fields, scenario 10 (5,000 iterations and 20 candidates) returned better results than scenario 11 (10,000 iterations and 100 candidates). The largest tested field, field Gert, with more than three times the number of field paths of the other three fields, was the only field where 100 candidates improved the results compared to 20 candidates. These results suggest that each field size has an optimal number of candidates, and that this number is larger for larger fields. Unfortunately, no research was found to support this suggestion.

Furthermore, Table 11 shows interesting results on computing times. The resulting average computing times are closely related to the number of iterations multiplied with the number of candidates. For scenarios 1 to 3 this multiplication is constant and equal to 1,000, whereas for scenario 4 this multiplication is equal to 4,000, thus four times as high. When comparing the computing times, the table shows that in all fields the average computing time for scenario 4 is

close to the four times as high as the computing times for scenarios 1 to 3. The same counts for scenario 11, where the multiplication of the number of iterations and the number of candidates is ten times as high as for scenario 10, and the average computing times per field for scenario 11 are also close to ten times as high as for scenario 10. This can be explained by the methods of the Tabu search algorithm (Figure 10); for every iteration a number of routes is calculated, equal to the number of candidates. The total number of routes calculated in one run is thus equal to the number of iterations multiplied with the number of candidates. Assuming a constant computing time per route calculation, it makes sense that the total computing time is directly related to this multiplication. Cordeau et al. (2001) performed a research using the Tabu search algorithm to solve a specific type of the VRP. They also found that computing times were directly proportional to the number of calculations performed within a run of the algorithm.

4.3 Test-cases

The objective function and optimization algorithm were tested on three test-case fields, based on data measured by farmers during capacitated field operations of planting potatoes. Optimized routes were compared to the routes chosen by the farmers. Results are shown in Table 11 and section 3.3. For all three test-case fields, the optimization algorithm found numerous routes with lower costs, measured by the objective function. When studying the resulting routes in detail (Figure 19), it stands out that with the basic weighting scheme scenario the spraypaths were suggested to be worked soon after a depot visit. This makes sense, since compaction in the spraypaths is deemed less important than compaction in normal field paths. Short after a depot visit, the weight of a working unit is at its highest (that is for application operations), and by working the spraypaths first the largest impact on soil compaction is found in the least important paths.

For field Korsendonk (Figure 19 c & d) the paths through the wet area are suggested to be worked shorter before a next depot visit, compared to the route chosen by the farmer. This counts in particular for the two paths with the longest distance through the wet area, with the highest impact on soil compaction. For Test field 2 (not shown) all paths through the wet area were also selected short before a depot visit, when the weight of the working unit is low. This is a desirable result, as minimizing compaction in wet areas was one of the main goals of this study, because of the higher susceptibility to soil compaction. However, in field Cools the field paths through the wet area were planned to be worked shorter after a depot visit in the optimized route, compared to the route chosen by the farmer, thus with a higher weight. This unexpected result was thought to be caused by a fault in the optimization part of the Python scripts. The far lower costs of the optimized route, compared to the route chosen by the farmer, opposes this assumption. This leaves only the explanation that the wet area had a very small impact on the route owing to its relatively small size. Unfortunately, these findings could not be compared to results in other researches, due to lack of comparable research.

The optimized routes suggested to work the fields in an unordered way, compared to the routes chosen by the farmers, where the paths were worked in order from one side of the field to the other side (section 3.3). The farmers thereby worked the fields in a sub-optimal but easy and clear order. For farmer Jacob van den Borne, the reason behind this was his personal preference for X-turns (personal communication, February 16, 2018). For farmer Gert Oudijk, the main reason behind this was that he believes that the impact of the weight of the potato planting machine on soil compaction is negligible (personal communication, February 9, 2018). In light of these opinions, regularly ordered routes were preferred, due to ease of planning. However, the results of the carried out test-cases suggest that routes with a different order would lead to less soil compaction.

A downside to the used methods is that the depot locations were no input data for the test-cases. This was due to the fact that the farmers moved the depots, and did not know the exact used locations anymore. Therefore, the depot locations were picked as practical locations, on the side of a road or farmhouse and easily reachable from numerous field paths. The actual depot locations might however have been different. These are not fixed but flexible, and might thus have been on more and different places. When and where depots are visited during a route chosen by the farmers was unknown. The created depot locations and the rule when to visit a depot might have negatively influenced the weightmeters of the route chosen by the farmer. It is important to keep this in mind when inspecting the results.

5 Conclusions and recommendations

In conclusion, this study proposed a method to determine an optimal route for capacitated agricultural operations over predefined field tracks given local differences in susceptibility to compaction (e.g. wet spots). Although the methods are only applicable to normal-shaped fields with two headlands, and an optimal weighting scheme for the objective function is yet to be researched, the method successfully incorporates the total weight of a working unit, wet spots in the field, bunker capacity, and induced soil compaction values for different movements.

- What defines an optimal route?
  An optimal route is defined as the route with minimal induced soil compaction. The total cost of a route is calculated in weightmeters [m*kg], defining the optimality of the route with regard to soil compaction.

- What optimization algorithm is best suited?
  A Tabu search algorithm is selected as best suited optimization algorithm, and is successfully implemented to optimize the search for a near-optimal route. In a small test field, this algorithm reached search times of 15.2% of the search time of an exhaustive search approach.

- Do test-case results show an improvement over conventional routing?
  In three test-cases, the defined route optimization method found routes that where more optimal than the routes chosen by farmers for a potato planting operation, with far lower costs in weightmeters.

Further research should be conducted to identify weighting schemes in accordance with induced soil compaction, e.g. the influence of turning movements compared to straight movements. The weighting schemes for the objective function are this far based solely on importance of different parts of fields and different types of movements, and on assumed relative impact on soil compaction.

In the current study, the only areas considered to have a higher susceptibility to soil compaction are discrete wet areas. In future research, the proposed algorithm could be improved by incorporating continuous input data on susceptibility to soil compaction. Studies on trafficability of soils and soil stress should be investigated for this purpose. Examples are e.g. Horn and Fleige (2003) and Duttmann et al. (2014).

The choice when to visit a depot is of major impact for the costs of a route. The route optimization algorithm could be improved by incorporating a decision mechanism on when to visit a depot. It is recommended to study the implementation of such mechanism in the algorithm in a following research.

Another recommendation for future research is on field path planning; once areas are known to be more susceptible to soil compaction, path planning methods could incorporate this by planning the spraypaths, which are the most trafficked field paths, outside of these areas. This way the spraypaths could still be used as main trafficking paths, without further deteriorating soil compaction in the susceptible areas. Numerous researches on path planning were analyzed (e.g. Oksanen and Visala (2007); de Bruin et al. (2014); Zhou et al. (2014)). However, no research was found that incorporates areas with higher soil vulnerability in path planning.

Results indicated that each field size might have an optimal number of candidates, and that this number is larger for larger fields. This should be investigated in future research.

In a follow-up study the suggested methods should be tested in practice. Thus far the optimized paths have only been studied in theory, based mainly on the objective function. Creating a route for and testing a route on a real-life capacitated field operation would give important insight in the applicability of the methods in practice. Feedback from farmers on suggested routes could prove helpful in further implementations of the methods. Once the methods are tested in practice, the proposed methods could be applied to farming machinery that work with GPS and predefined field tracks. By planning routes ahead of an agricultural operation, the total costs in weightmeters and thus the induced soil compaction could be decreased in all tested scenarios.

6 Acknowledgements

References

Aliev, K.
   2001. Current problems with regard to mechanization and greening of farming in azerbaijan. *Mezhdunarodnyi Sel'skokhozyaistvennyi Zhurnal*, 5:57–61.

Altınel, İ. K. and T. Öncan
   2005. A new enhancement of the clarke and wright savings heuristic for the capacitated vehicle routing problem. *Journal of the Operational Research Society*, 56(8):954–961.

Baker, B. M. and M. Ayechew
   2003. A genetic algorithm for the vehicle routing problem. *Computers & Operations Research*, 30(5):787–800.

Bakhtiari, A. A., H. Navid, J. Mehri, and D. D. Bochtis
   2012. Optimal route planning of agricultural field operations using ant colony optimization. *Agricultural Engineering International: CIGR Journal*, 13(4).

Bakker, D. and R. Davis
   1995. Soil deformation observations in a vertisol under field traffic. *Soil Research*, 33(5):817–832.

Barbarosoglu, G. and D. Ozgur
   1999. A tabu search algorithm for the vehicle routing problem. *Computers & Operations Research*, 26(3):255–270.

Bell, J. E. and P. R. McMullen
   2004. Ant colony optimization techniques for the vehicle routing problem. *Advanced engineering informatics*, 18(1):41–48.

Bochtis, D. and S. Vougioukas
   2008. Minimising the non-working distance travelled by machines operating in a headland field pattern. *Biosystems engineering*, 101(1):1–12.

Boguzas, V., I. Hakansson, et al.
   2001. Barley yield losses simulation under lithuanian conditions using the swedish soil compaction model. In *Conference on sustainable agriculture in Baltic States, Tartu (Estonia), 28-30 Jun 2001*. Tartumaa Ltd.

Braunack, M., J. McPhee, and D. Reid
   1995. Controlled traffic to increase productivity of irrigated row crops in the semi-arid tropics. *Australian Journal of Experimental Agriculture*, 35(4):503–513.

Brownlee, J.
   2011. *Clever algorithms: nature-inspired programming recipes*. Jason Brownlee.

Chygarev, Y., S. Lodyata, et al.
   2000. Research of tyre rigidity in terms of ecological safety of agricultural landscapes. *VII Międzynarodowe Sympozjum Ekologiczne Aspekty Mechanizacji Nawożenia, Ochrony Roślin Uprawy Gleby i Zbioru Roślin Uprawnych, Warsawa, Poland, 18-19 wrzesien 2000*, Pp. 171–176.

Cordeau, J.-F. and G. Laporte
   2005. Tabu search heuristics for the vehicle routing problem. *Metaheuristic Optimization via Memory and Evolution*, Pp. 145–163.

Cordeau, J.-F., G. Laporte, and A. Mercier
   2001. A unified tabu search heuristic for vehicle routing problems with time windows. *Journal of the Operational research society*, 52(8):928–936.

Dantzig, G. B. and J. H. Ramser
   1959. The truck dispatching problem. *Management science*, 6(1):80–91.

de Bruin, S., P. Lerink, I. J. La Riviere, and B. Vanmeulebrouk
   2014. Systematic planning and cultivation of agricultural fields using a geo-spatial arable field optimization service: Opportunities and obstacles. *Biosystems engineering*, 120:15–24.

Douglas, J.
  1994. Responses of perennial forage crops to soil compaction. *Developments in Agricultural Engineering*, 11:343–364.

Duttmann, R., M. Schwanebeck, M. Nolde, and R. Horn
  2014. Predicting soil compaction risks related to field traffic during silage maize harvest. *Soil Science Society of America Journal*, 78(2):408–421.

Gan-Mor, S. and R. L. Clark
  2001. Dgps-based automatic guidance–implementation and economical analysis. In *2001 ASAE Annual Meeting*, P. 1. American Society of Agricultural and Biological Engineers.

Gliński, J., J. Lipiec, et al.
  1990. *Soil physical conditions and plant growth*. CRC Press Inc.

Greene, W. D. and W. B. Stuart
  1985. Skidder and tire size effects on soil compaction. *Southern Journal of Applied Forestry*, 9(3):154–157.

Hamza, M. and W. Anderson
  2005. Soil compaction in cropping systems: a review of the nature, causes and possible solutions. *Soil and tillage research*, 82(2):121–145.

Hetz, E.
  2001. Soil compaction potential of tractors and other heavy agricultural machines used in chile. *Agricultural mechanization in asia africa and latin america*, 32(3):38–42.

Horn, R. and H. Fleige
  2003. A method for assessing the impact of load on mechanical stability and on physical properties of soils. *Soil and Tillage Research*, 73(1-2):89–99.

Jensen, M. A. F., D. Bochtis, C. G. Sørensen, M. R. Blas, and K. L. Lykkegaard
  2012. In-field and inter-field path planning for agricultural transport units. *Computers & Industrial Engineering*, 63(4):1054–1061.

Jensen, M. F., D. Bochtis, and C. G. Sørensen
  2015a. Coverage planning for capacitated field operations, part ii: Optimisation. *Biosystems Engineering*, 139:149–164.

Jensen, M. F., M. Nørremark, P. Busato, C. G. Sørensen, and D. Bochtis
  2015b. Coverage planning for capacitated field operations, part i: Task decomposition. *biosystems engineering*, 139:136–148.

Kutzbach, H. D.
  2000. Trends in power and machinery. *Journal of Agricultural Engineering Research*, 76(3):237–247.

Laporte, G.
  1992. The vehicle routing problem: An overview of exact and approximate algorithms. *European journal of operational research*, 59(3):345–358.

Laporte, G., M. Gendreau, J.-Y. Potvin, and F. Semet
  2000. Classical and modern heuristics for the vehicle routing problem. *International transactions in operational research*, 7(4-5):285–300.

Li, Y., J. Tullberg, D. Freebairn, and H. Li
  2009. Functional relationships between soil water infiltration and wheeling and rainfall energy. *Soil and Tillage Research*, 104(1):156–163.

Lipiec, J., A. Ferrero, V. Giovanetti, A. Nosalewicz, and M. Turski
  2002. Response of structure to simulated trampling of woodland soil. *Adv. Geoecol*, 35:133–140.

Lipiec, J. and C. Simota
  1994. Role of soil and climate factors in influencing crop responses to soil compaction in central and eastern europe. *Developments in agricultural engineering*, 11:365–390.

McGarry, D.
  2003. Tillage and soil compaction. *Conservation agriculture*, Pp. 307–316.

McPhee, J., P. Aird, M. Hardie, and S. Corkrey
  2015. The effect of controlled traffic on soil physical properties and tillage requirements for vegetable production. *Soil and Tillage Research*, 149:33–45.

Oksanen, T. and A. Visala
  2007. *Path planning algorithms for agricultural field machines*. Helsinki University of Technology.

Oldeman, L.
  1992. Global extent of soil degradation. *Bi-Annual Report 1991-1992/ISRIC*, Pp. 19–36.

Palmer, R., D. Wild, and K. Runtz
  2003. Improving the efficiency of field operations. *Biosystems engineering*, 84(3):283–288.

Panyam, S.
  . Clever algorithms in python. `http://www.saipanyam.net/code-center/clever-algorithms-in-python`. Accessed: Dec. 22, 2017.

Ridge, R.
  2002. Trends in sugar cane mechanization. *International sugar journal*, 104(1240):164–166.

Sabelhaus, D., F. Röben, L. P. M. zu Helligen, and P. S. Lammers
  2013. Using continuous-curvature paths to generate feasible headland turn manoeuvres. *Biosystems Engineering*, 116(4):399–409.

Soane, B., J. Dickson, and D. Campbell
  1982. Compaction by agricultural vehicles: A review iii. incidence and control of compaction in crop production. *Soil and tillage research*, 2(1):3–36.

Soane, B. and C. Van Ouwerkerk
  1994. Soil compaction problems in world agriculture. *Developments in agricultural engineering*, 11:1–21.

Spekken, M. and S. de Bruin
  2013. Optimized routing on agricultural fields by minimizing maneuvering and servicing time. *Precision agriculture*, 14(2):224–244.

Spekken, M. and J. Molin
  2012. Optimizing path planning by avoiding short corner tracks. In *Proceedings of the 11th international conference on precision agriculture. Indianapolis, IN: EUA.*

Taïx, M., P. Souères, H. Frayssinet, and L. Cordesses
  2003. Path planning for complete coverage with agricultural machines. *Field and service robotics*, Pp. 549–558.

Tullberg, J., D. L. Antille, C. Bluett, J. Eberhard, and C. Scheer
  2018. Controlled traffic farming effects on soil emissions of nitrous oxide and methane. *Soil and Tillage Research*, 176:18–25.

Tullberg, J., D. Yule, and D. McGarry
  2007. Controlled traffic farming—from research to adoption in australia. *Soil and Tillage Research*, 97(2):272–281.

Veen, B., M. Van Noordwijk, P. De Willigen, F. Boone, and M. Kooistra
  1992. Root-soil contact of maize, as measured by a thin-section technique. *Plant and Soil*, 139(1):131–138.

Zhou, K., A. L. Jensen, C. G. Sørensen, P. Busato, and D. Bothtis
  2014. Agricultural operations planning in fields with multiple obstacle areas. *Computers and Electronics in Agriculture*, 109:12–22.